Aus dem Neurowissenschaftlichen Forschungszentrum
der Medizinischen Fakultät Charité – Universitätsmedizin Berlin

DISSERTATION

SENSORY AND ASSOCIATIVE MICROCIRCUITS IN THE OLFACTORY CORTEX

zur Erlangung des akademischen Grades
Medical Doctor – Doctor of Philosophy (MD/PhD)
im Rahmen des International Graduate Program Medical Neurosciences

vorgelegt der Medizinischen Fakultät Charité – Universitätsmedizin Berlin
von

Hauke Felix Wiegand
aus Achim, Niedersachsen, Deutschland

Gutachter/in: 1. Prof. Dr. D. Schmitz
2. Prof. Dr. M. P. Nawrot
3. Prof. Dr. M. Larkum

Datum der Promotion: 23.06.2013

Acknowledgements

I would like to thank:

Dietmar Schmitz and Friedrich Johenning for being so present as supervisors, always open to questions and suggestions, and paying attention not only to the project but the preferences and individuality of the lab members,

Prateep Beed, Christian Leibold and Michael Bendels for the constructive cooperation and many explanations in data analysis,

Claudia Böhm and Moritz Wigand for critical reading of this thesis,

Anke Schönherr und Susanne Walden for very helpful technical assistance,

and the Schmitzlab crew for the always friendly and cooperative atmosphere in the lab.

1 TABLE OF CONTENTS

1 Table of Contents 4
2 List of Figures and Tables 6
3 Abbreviations 7
4 Introduction 9
4.1 The mammalian olfactory system 10
4.2 The Piriform Cortex 13
4.2.1 Horizontal organization 13
4.2.2 Anterior-posterior and dorsal-ventral organization 14
4.2.3 Olfactory coding 15
4.2.4 Plasticity 17
4.2.5 Oscillations 18
4.2.6 Inputs and Outputs 19
4.3 Diseases affecting the olfactory system 20
4.4 Cell Type Specific Subcircuits – Hypothesis 21
5 Methods 23
5.1 Experimental Procedures 23
5.1.1 Slice Preparation 23
5.1.2 Electrophysiology 23
5.1.3 Glutamate uncaging and scanning of glutamate-evoked activity 24
5.1.4 Histological procedures 26
5.1.5 Two-Photon Calcium Imaging (TPCI) 27
5.2 Data analysis and statistics 28
5.2.1 Analysis of LSPS data 29
5.2.2 Analysis of Population Calcium Imaging Data 30
5.2.3 Statistics 31
6 Results 32
6.1 Cell Types and Calibration 32
6.1.1 Principle Cell Types in the Piriform Cortex 32

6.1.2 Calibration of Spatial Resolution 35
6.2 Probing associative inputs by LSPS 37
6.2.1 Generation of principal cell-type specific afferent input maps from different APC layers 37
6.2.2 L2S, L2Ps and L3Ps: comparison of intracortical connectivity 40
6.2.3 Layer III pyramidal cells: dorsal-ventral asymmetry of recurrent feedback excitation 43
6.3 Analysis of sensory input by fast TPCI reveals stronger recruitment of superficial layer II cells 45
7 Discussion 49
7.1 Limitations 49
7.2 The organization of intracortical and sensory circuits in aPC layer II can be described as a converse gradient 50
7.3 Specialized superficial microcircuits 51
7.4 Output firing, cortical odour coding, plasticity 52
7.5 Intracortical connections along the dorso-ventral axis: Asymmetry and the role of deep cells 53
7.6 An updated (and speculative) PC network model 54
8 Summary/Abstract 59
9 Literature 60
10 Selbständigkeitserklärung 70
11 Curriculum Vitae 71
12 Publikationen und Poster 74

2 LIST OF FIGURES AND TABLES

Figure 1 – Location and structure of the PC 12
Figure 2 – slicing plane 23
Figure 3 – laser scanning photostimulation setup 25
Figure 4 – Inhibitory effect of MNI-Glutamate 26
Figure 5 – two-photon population imaging setup 28
Figure 6 – Biocytin reconstructions and Input-Output-Curves demonstrating the vertical transition 32
Figure 7 – aPC principal cells are organized in a continuous gradient 35
Figure 8 – Resolution of photoactivation by glutamate uncaging 36
Figure 9 – Mapping local recurrent feedback excitation 39
Figure 10 – L2S and L2P example maps 41
Figure 11 – Intracortical connectivity increases from superficial to deep 42
Figure 12 – L3Ps receive asymmetric inputs on the ventrodorsal axis 44
Figure 13 – Single cell excitability probing of sensory layer Ia inputs to deep and superficial layer II neurons by fast TPCI 46
Figure 14 – Schematic aPC circuit diagram 56

3 ABBREVIATIONS

AMPAR	–	α-amino-3-hydroxy-5-methyl-4-isoxazolepropionic acid receptor
AP	–	action potential
aPC	–	anterior piriform cortex
EPSC	–	excitatory postsynaptic current
EPSP	–	excitatory postsynaptic potential
DL2	–	deep layer II cell
GABA	–	gamma amino buteric acid
IPSC	–	inhibitory postsynaptic current
IPSP	–	inhibitory postsynaptic potential
L2P	–	layer II superficial pyramidal cell
L2S	–	layer II semilunar cell
L3M	–	layer III multipolar cell
L3P	–	layer II deep pyramidal cell
LOT	–	lateral olfactory tract
LSPS	–	laser scanning photo stimulation
LTD	–	long term depression
LTP	–	long term potentiation
M and T cells	–	mitral and tufted cells
NMDAR	–	N-methyl D-aspartate receptor
OB	–	olfactory bulb
PC	–	piriform cortex
pPC	–	posterior piriform cortex
PSC	–	postsynaptic current
SD	–	standard deviation
SEM	–	standard error of the mean
SL2	–	superficial layer II cell
SWR	–	sharp wave ripples
TPCI	–	two-photon-Calcium-Imaging

„Grenouille aber roch alles wie zum ersten Mal. Und er roch nicht nur die Gesamtheit dieses Duftgemenges, sondern er spaltete es analytisch auf in seine kleinsten und entferntesten Teile und Teilchen. Seine feine Nase entwirrte das Knäuel aus Dunst und Gestank zu einzelnen Fäden von Grundgerüchen, die nicht mehr weiter zerlegbar waren. “

Patrick Süßkind, Das Parfüm

4 INTRODUCTION

The olfactory system of mammals is specialized to detect odours, to form and recognize olfactory objects and to link them to other modalities and behaviour. This is a complex and important task: Real-world aromas are complex mixtures of odorant molecules that contain information about pleasures, dangers, attractive and aversive properties of the surrounding world – like quality, condition and location of food – and about other creatures – like dangerous predators, rivalling fellows and potential partners. Probably, more than 400 000 different substances are perceptible as odours for humans and many more for some other animal species (Nagao et al., 2002). Relevant odours have to be discriminated from a "noisy" background. This is challenging, as they are varying in their quantitative presentation through variables like wind direction, humidity and air temperature and in their qualitative chemical signature, as the chemical composition emitted by an odour source may vary through time by ecological factors like dilapidation. In addition to the constant processing of odours from the surrounding environment, many species actively sniff at their environment, thereby allowing for a defined timing and localization of the perceived odours (Gottfried, 2010).

How can we understand at least in part how the olfactory system tackles this challenge? The olfactory system is a sensory system and part of the mammalian central nervous system. Of course, it is impossible to describe state and development of every single element of the system, as this would overtax both our own cognitive capacities as well as the computation capacity of today's computer systems (Douglas and Martin, 2007). Instead, in order to 'understand' such a (neuro-) biological system, one can try to define forms of appearance, principles of organization and laws and rules of dynamic change that relate to known concepts. In neurobiology such definitions are made on different levels of description: Macroanatomy and topographical anatomy describe forms, structures and their relations delimitable with the naked eye. Histology characterizes the cell types that compose a tissue and their structural composition. Microanatomy relates these descriptions to the macroanatomically visible forms and structures. Physiology

describes dynamic properties of biological systems and tries to define laws and rules in the language of physics and biochemistry. Functional anatomy links anatomical organization to physiological function. Behavioural sciences systematically analyze activities in defined situations and interactions among organisms. In order to find principles of form, organization and function that are not immediately falsifiable (Popper, 2002) one has to generalize and thereby reduce complexity.

In this work I will describe our research on the principles of connectivity and processing of information by classes of cell types in the piriform cortex (PC), the largest part of the olfactory system. As a model system we were working in slices of rat brains. In our work we thus tried to find principles of organization and function on the level of functional microanatomy. In order to understand the motivation for this choice and the relevance of our findings, I will first give a short introduction to the anatomical structure and coarse function of the olfactory system and then describe functional microanatomical characteristics of the PC more in detail. If not otherwise indicated, I cite studies done in rodents.

4.1 The mammalian olfactory system

In humans and rodents, odours are detected by olfactory sensory neurons in the olfactory epithelium in the nose. Odour molecules bind to odorant receptors on the surface of these cells. Individual sensory neurons are equipped only with one type of odorant receptor. However, they can respond to a range of odour molecules with different affinities. Vice versa, a distinct odour molecule mostly activates many different receptors with varying efficacies (Murthy, 2011). Olfactory sensory neurons project exclusively to the olfactory bulb (OB), the first processing stage in the olfactory system. Their axons converge onto structures called “glomeruli”, a kind of first signal processing module in the OB (Mori et al, 1999). A single glomerulus receives input only from sensory neurons expressing the same receptor type (Murthy, 2011). In a glomerus the axons of olfactory sensory neurons contact different targets: They make connections with excitatory glutamatergic mitral and tufted cells (M and T cells) that are the major output

neurons of the OB, and with diverse classes of GABAergic, glutamatergic and dopaminergic juxtaglomerular neurons. The largest neuron population in the OB are granule cells that receive inputs from M and T cells and backprojections from cortical neurons. A part of the granule cell and juxtaglomerula cell population is subject to a continuous turnover, whereby newborn and more plastic cells get integrated into the existing circuitry (Isaacson, 2010, Lazarini and Lledo, 2011).

The OB M and T output neurons are connected to higher cortical areas. Olfactory cortices are areas in the basal frontal and medial temporal lobes of the brain that receive direct input from the OB. In contrast to the processing of information from other senses, such as vision, audition or somatosensation, the thalamus does not serve as a relay between the cortex and the periphery. Some authors speculate that the OB is fulfilling the function that the thalamus serves in other sensory systems (Gottfried, 2010). Additionally, no clear hierarchical and functional order of cortical regions (like V1, V2, V3, V4 in the visual cortex) can be found. On the basis of macro- and mircoanatomical properties olfactory cortical areas can be distinguished, but their relation is unclear (Fig. 1A). The largest area is the piriform cortex (PC), which receives strong input from the OB via the lateral olfactory tract (LOT). Based on axonal connections and cytoarchitectural properties different subregions of the PC can be described: The anterior piriform cortex (aPC) has a ventral subdivision covered by the superficial LOT fiber bundle and a dorsal subdivision dorsal to the LOT, whereas the posterior piriform cortex (pPC) is situated posterior to the LOT (Fig. 1A) (Nevile and Haberly, 2004).

Which broad behavioural functions can the olfactory areas be linked to? It has been suggested that the glomerular structure of the OB that bundles information from different olfactory sensory neurons and distributes it to the cortex serves as a kind of "information look up table" (Isaacson, 2010). Periglomerular cells and granule cells modify M and T cell output, thereby sharpening contrasts and controlling output gain (Lazarini and Lledo, 2011; Isaacson, 2010). The anterior olfactory nucleus (Fig. 1A) is involved in interhemispheric information exchange and coordination (Brunjes et al., 2005; Illig and Eudy, 2009), whereas the functions of the tenia tecta and the peduncular cortex in olfaction remain unknown. The function of the PC is still under debate: On the one hand, it is the primary olfactory

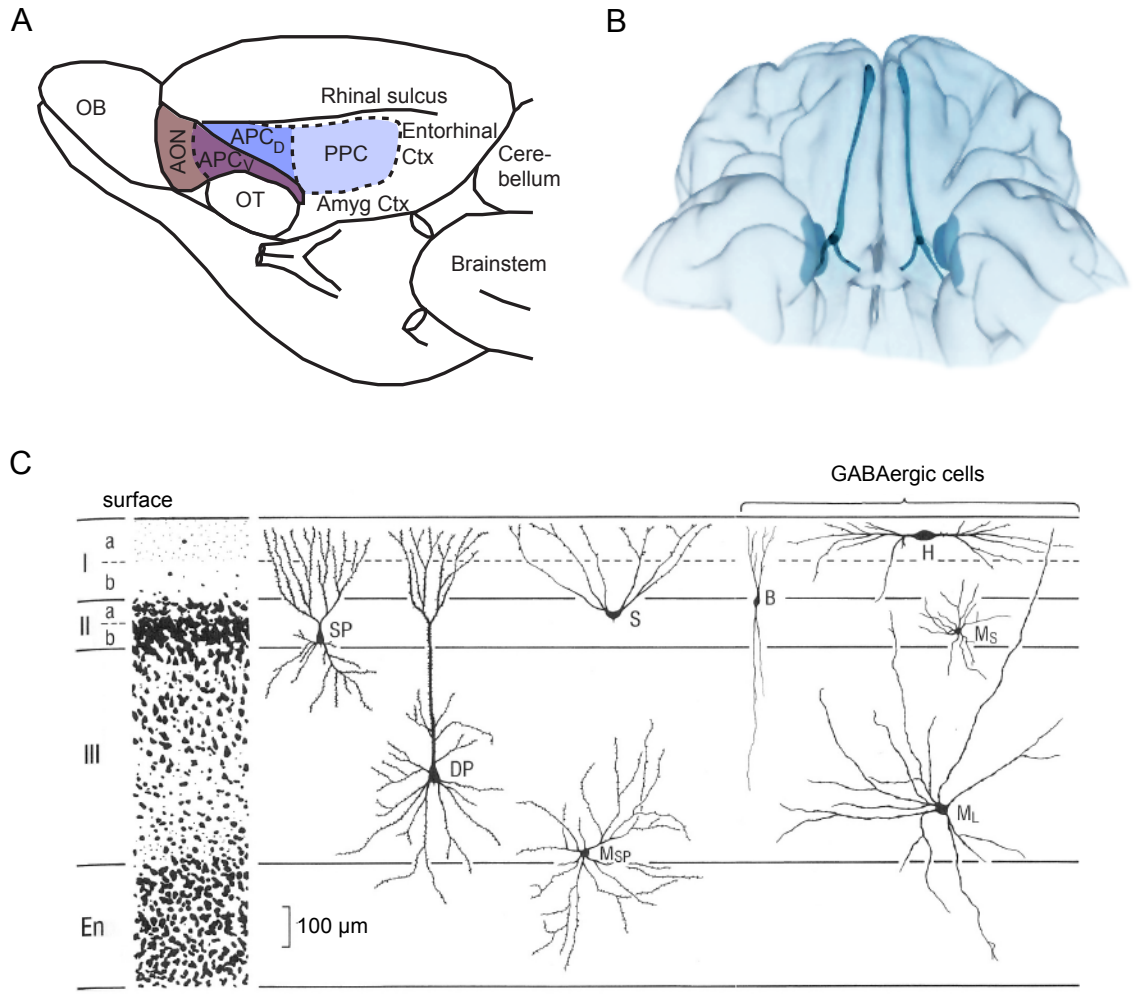

Figure 1 *– Location and structure of the PC*

A and B Sketches of an isolated rodent (A) and human (B) brain. The first processing station of olfactory information is the olfactory bulb (OB). Via the LOT (violet) axons from OB cells reach the piriform cortex (PC, blue; parts covered by the LOT in dark violet) that constitutes the largest part of the olfactory cortex. Anatomically, several subdivisions can distinguished: The anterior piriform cortex (aPC) has a ventral subdivision deep to the LOT and a dorsal subdivision dorsal to the LOT, whereas the posterior piriform cortex (pPC) is situated posterior to the LOT and has a prominent layer III. Higher areas engaged in olfactory processing are the orbitofrontal cortex, amygdala, perirhinal cortex and entorhinal cortex.

C Layering of the PC: As a phylogenetically old paleocortex, PC shows a three-layerd structure. Layer Ia contains fibers transmitting exclusively sensory information from the OB. Layer Ib consists of both local and long-range associative fibers. Layer I and II horizontal and neurogliaform cells are implied in early feedforward inhibition, layer II and III neurogliaform and inhibitory multipolar cells in late perisomatic inhibition. Current descriptions described so far semilunar and superficial pyramidal cells as two different excitatory cell populations in layer II. Layer III contains deep pyramidal cells and spiny multipolar cells as excitatory neurons. Deep to layer III lays the endopiriform nucleus with predominantly multipolar cells.

A modified from Ekstrand et al., 2001; B modified from http://dasgehirn.info /entdecken/anatomie/der-paleocortex/; (C) modified from Neville and Haberly, 2004.

cortex and was thus seen analogous to other primary sensory areas as a feedforward sensory processing module, on the other hand it shows typical characteristics of associative cortices (see 4.4). Functional magnetic resonance imaging studies in humans imply that odour background differentiation is processed by the OB and the aPC. Representations of the chemical identity of the components of an odour (like 'ethyl acetate, α-farnesene and butanol') are found in the aPC, whereas the pPC is coding its perceptual quality (like 'pear' for the before mentioned substances). Perceptual and associative learning, attention selection and conscious odour perception rely on pPC and orbitofrontal cortex networks (Gottfried, 2011).

4.2 The Piriform Cortex

4.2.1 Horizontal organization

The PC has a three-layer laminar organisation (Fig. 1C and 12D) in its vertical plane – another important difference of this palaeocortical system from sensory systems that emerged later in evolution and that have a six-layered neocortical vertical structure:

The superficial plexiform layer I contains dendrites, fibre systems, and only a small number of neurons. These are mainly interneurons called horizontal cells. Its superficial part, layer Ia, receives exclusively sensory olfactory bulb input via the LOT, its deep part, layer Ib, consists of corticocortical association fibers from other olfactory cortical areas and the PC itself (Neville and Haberly, 2004; Suzuki and Bekkers, 2010).

Layer II is a compact layer containing cell bodies and associational fibers. Current descriptions propose two separate populations of excitatory cells: in the superficial part semilunar cells, that lack basal dendrites and have apical dendrites with two major branches (Fig.1C) and large spines primarily located in layer Ia and in its deep part pyramidal cells. Apical dendrites of these layer II superficial pyramidal cells extend to layer Ia, and for the majority of cells, basal dendrites extend into layer III. Semilunar cells get nonfacilitating sensory excitatory inputs and fire nonbursting action potentials (APs) that are followed by a strong

afterhyperpolarization. Depending on the strength of input, they tend to fire output APs at frequencys < 40 Hz. Superficial pyramidal cells receive heavily facilitating sensory inputs and produce bursts of APs. They tend to fire at frequencies > 40 Hz (Suzuki and Bekkers, 2006). It is important to note that Suzuki and Bekkers compared cells at extreme spatial locations: a semilunar population at the border to layer I and a pyramidal cell population close to the border to layer III, but probably they did not sample any neurons in the intermediate part.

Layer III in its superficial part contains mainly pyramidal cells. These deep pyramidal cells have dendrites extending to layer Ia, too. In their electrophysiological properties they differ from superficial pyramidal cells, for example by having a lower spike threshold (Neville and Hyberly, 2004). In the deep part of layer III, large GABAergic inhibitory multipolar cells and a smaller number of spiny excitatory multipolar cells are the principal neurons. Deep in the cortex, under dorsal parts of layer III the endopiriform nucleus can be found that is termed by some authors layer IV. Here the predominant excitatory cell type are spiny excitatory multipolar neurons (Neville and Haberly, 2004).

Several classes of structurally different inhibitory cell types exist in the piriform cortex: horizontal and neurogliaform cells in layer I and II, bitufted cells in layer II and neurogliaform and fast-spiking- and regular-spiking inhibitory multipolar cells in layer III (Neville and Haberly 2004, Suzuki and Bekkers, 2010; Fig. 1C).

4.2.2 Anterior-posterior and dorsal-ventral organization

Whereas the PC shows a clear vertical laminar organisation, the horizontal structure is much more diffuse:

First, the thickness of layer Ib (thus the strength of the associative input fibre bundle) in comparison to Ia (the sensory input fibre bundle) increases from anterior to posterior, thus from APC to PPC, and from ventral to dorsal in the APC (Neville and Haberly, 2004). Second, the area of termination of intrinsic association fibres in the horizontal laminar organisation depends on their area of origin, and, furthermore, appears to follow the sequence of activation of the different subregions. For example, association projections from ventral APC are only in the

superficial part of layer Ib throughout all the other PC, whereas association connections from dorsal APC synapse rather in middle parts of Ib, and fibers from PPC mostly terminate in layer III (Neville and Haberly, 2004). Third, aPC inhibitory inputs to pyramidal cells are asymmetrically organized with a posterior shift on the anterior-posterior axis (Luna and Pettit, 2010). Fourth, associational projections (as well as commissural projections) between the different PC subregions show a clear asymmetry. For example, projections from ventral APC to dorsal APC and from APC to PPC are mainly one-way connections (Neville and Haberly 2004). Afferent input to the PPC is much more broadly distributed than in APC. In functional experiments higher concentrated odorants activate larger regions of the cortex, and anterior sites show lower activation thresholds than posterior sites. In response to defined odorants, individual PPC cells seem to be more selective than cells in the APC (Sugai et al., 2005; Wilson et al., 2006).

4.2.3 Olfactory coding

How do these structures and the different cell types contribute to the coding of olfactory information? M and T cell axons from the olfactory bulb glomeruli synapse exclusively in layer Ia on dendrites of layer II excitatory cells and interneurons. Whereas the OB shows a clear "recepterotopic" spatial arrangement of inputs, PC activation by sensory inputs seems to follow different organisation principles:

Different odorants seem to activate 3–15% of the superficial excitatory cell population in the aPC. Each odorant activates distinct but overlapping cell ensembles that show no spatial clustering (Illig and Haberly, 2003; Rennacker et al., 2007; Stettler and Axel, 2009; Poo and Isaacson, 2009; Apicella et al., 2010). An interesting additional finding is that olfactory cortical ensembles activated in response to complex mixtures of odorants are invariant to small variations in their composition (as is the related behavioural performance). Therefore they may function as a kind of pattern completion mechanism that allows perceptual stability (Barnes et al., 2008).

OB and PCX principle cells have no "exclusive" connections: genetic tracing studies

showed that individual cortical excitatory cells receive input from on average at least four M/T cells. At the same time, M and T cells getting input from the same glomerulus project independently to different PC neurons (Miyamchi et al, 2011). In an in vivo imaging study individual cells responded to several, even structurally different odorants and a subpopulation of cells responded only to mixtures of odorants but not to their components (Stettler and Axel, 2009). The response to increasing odorant concentrations does not increase linearly with the concentration but saturates (Stettler and Axel, 2009).

"Global inhibition" is tuning the dispersed activity in the highly associative network to the locally sparse and temporally precise ensemble coding. "Global inhibition" thereby means a widespread and nonselective suppression of excitation by inhibtion (Poo and Isaacson, 2009). Different inhibitory circuits can be distinguished that fall into two broad classes: Dendritic feedforward and somatic feedback inhibition.

Feedforward apical dendritic inhibition is mediated by layer I horizontal and neurogliaform cells. Horizontal cells are found only close to the LOT, whereas neurogliaform cells are widely distributed throughout layer I (Suzuki and Bekkers, 2010 and 2012). These feedforward interneurons receive input from a broader set of glomeruli than excitatory neurons and the synapses between M and T cells and feedforward interneurons have a higher release probability then contacts between M and T cells and excitatory cells. It is speculated that feedforward inhibition in PC acts as a kind of "salience filter" that can be overcome only by strong burst inputs (Stokes and Isaacson, 2010; Suzuki and Bekkers, 2012). It is most effective when M and T cells fire sparsely. However, when bursts of sensory input by M and T cells arrive, it wanes strongly, a mechanism that allows activation of excitatory cells (Stokes and Isaacson, 2010).

Instead, by this stronger excitation, somatic feedback inhibition is recruited, but follows later in bursts of input. It leaves open a 2-10 ms time window for output firing of excitatory cells (Luna and Schoppa, 2008; Stokes and Isaacson, 2010). This inhibitory feedback mechanism might be provided by layer 3 interneurons, thus neurogliaform, bitufted, fast-spiking inhibitory multipolar and regular-spiking inhibitory multipolar cells (Suzuki and Bekkers, 2010 and 2012) (Fig. 1C and 12D).

These neurons make connections with a large fraction of neighbouring pyramidal cells so that it is speculated that they may be implied in "lateral inhibition" mechanisms (Stokes and Isaacson, 2010).

A detailed quantification of synaptic contacts originating from single superficial layer II pyramidal cells reveals an even distribution of long-range connections in the piriform cortex without a tendency towards a stereotype local clustering (Illig and Haberly, 2003). However, local collateral regions of intense axonal branching around the pyramidal cell body were found, too (Johnson et al., 2000). This hints at the existence of local associative microcircuits between principle excitatory piriform cortex neurons, but how these microcircuits are organized and what functional role they are playing was unclear so far.

4.2.4 Plasticity

The cell groups that are connected in microcircuits are not static hard-wired ensembles, but plasticity mechanisms allow dynamic changes in their modes of input processing, connectivity and output firing. Some authors relate synaptic and cellular plasticity to learning and memory phenomena (e.g. Malenka and Nicoll, 1997; Rogan et al. 1997; Best and Wilson, 2004). Dependent on timescale and synapse, different modes of plasticity are found in PC:

The M and T to pyramidal cell synapse shows short-term depression on a timescale of a minute. It is mediated at least in part by a presynaptic mechanism downstream of calcium influx and intracellular release (Wiegand et al, 2010) and can be influenced by presynaptic metabotropic glutamate receptors group III and beta-adrenergic receptors (Best and Wilson, 2004). It has been suggested that this mechanism mediates odour habituation, which can be observed on a behaviour level (Best and Wilson, 2004).

PC pyramidal cell dendrites possess two different compartments corresponding to the clear anatomical segregation of LOT and associative inputs: a more distal compartment where the sensory inputs synapse and a more proximal compartment where associative synapses are located. The associative synapses on L2P in layer Ib can undergo strong NMDA-dependent longterm potentiation (LTP)

(Kanter and Haberly, 1990; Quinlan et al., 2004; Franks and Isaacson, 2005), whereas in layer Ia M/T to pyramidal cell synapses LTP is not reliably or just very modestly inducible after a short critical period during development (Jung et al., 1990, Kanter and Haberly, 1990 and 1993). Several mechanistic explanations for the differences between layer Ia and layer Ib were found: First, LTP induction by pairing EPSPs with subsequent AP bursts under physiological conditions seems to be possible only in layer Ib mediated by much larger spine Ca^{2+} signals. The smaller layer Ia signals are partially due to a smaller VGCC mediated Ca^{2+} influx and a more robust Mg^{2+} block of the NMDAR (Johenning et al., 2009). Second, LTP expression in layer Ia is altered by an AMPAR/NMDAR ratio change dependent on olfactory experience (it can be prevented by a unilateral naris occlusion) during development towards a downregulation of NMDAR and a modest upregulation of AMPAR (Franks and Isaacson, 2005). Additionally, different forms of learning influence the composition of NMDARs, an important factor detemining LTP expression (Quinlan et al., 2004). The associative synapses on pyramidal cells are able to express long-term depression (LTD) in synaptic strength, too. It is unclear if pre- and postsynaptic mechanisms both play a role, but presynaptic metabotropic glutamate receptors seem to be involved (Young and Sun, 2007).

4.2.5 Oscillations

Not only the spatial organisation of a network but also temporal organisation patterns are crucial for information processing. In this regard network oscillations are important phenomena. In PC two basal oscillatory states have been described (local field potentials and single cell membrane potentials): Slow wave states (0,5-2 Hz), which can be found in many networks during natural sleep or deep anaesthesia, and faster beta (15-30 Hz) or theta frequency states (4-12 Hz,) which correspond to shallower states of anaesthesia or some forms of awake behaviour. During slow-wave sleep states sharp wave ripple complexes (SWR) can be observed, too, that are independent from hippocampal SWRs. APC generated SWRs drive OB SWRs and it is speculated that these oscillations contribute to the reorganisation of OB granule cell circuits (Manabe et al., 2011).

In contrast to OB neurons, the majority of PC neurons respond only during fast wave states to presented odours, but not during slow wave states (Murakami et al, 2005). These findings suggest, that the PC has a state-dependent gating function for the olfactory system, which is similar to parts of the thalamus in other sensory systems. It has been speculated, that the switch between slow and fast wave states is modulated by acetylcholine, which suppresses intrinsic association fiber synapses and thereby makes the system more sensitive to afferent activity (Hasselmo and Bower, 1992; Wilson and Yan, 2010).

During weak anaesthesia odours evoke respiration-coupled, beta-frequency oscillations in the PC local field potential: The firing activity of not specified single layer II/III cells is slowly modulated over time by respiration and precisely phase-locked to the local field potential beta oscillation. Oscillating excitation precedes inhibition by a few milliseconds, restricting spike timing to a brief temporal window. This allows precise spike timing despite the slow respiratory patterning and opens the possibility of a temporal dimension in odour coding (Poo and Isaacson, 2009).

A PC network isolated from the OB generates slow wave oscillations spontaneously, with up states and down states alternating at an average frequency of 1.8 Hz. These oscillations seem to be initiated at the border between layer III and the endopiriform nucleus (Sanchez-Vives et al, 2008), a region with highly excitable principle cells (Tseng and Hyberly, 1989a and 1989b) and very dense recurrent connections (Hoffman and Haberly, 1991 and 1993). The activity within slow-wave states is influenced by recent odour experience (Wilson, 2010) and more coherent with the activity of other cortical forebrain structures (Wilson and Yan, 2010).

4.2.6 Inputs and Outputs

The PC is highly interconnected with other brain areas, most of these inputs are not one-way connections but reciprocal: As mentioned before the primary sources of afferent input are olfactory bulb mitral cell axons, reaching the PC via the LOT. PC neurons project also back to the olfactory bulb, mainly to inhibitory granule cells

(Murthy, 2011). Via superficial and deep pyramidal cells as well as spiny multipolar cells, the piriform cortex is interconnected with other olfactory areas (both strong associational and less strong commissural projections) and higher cortical areas (Fig. 1A). That means, that olfactory information is linked to systems implied in memory formation and retrieval, affective learning, emotional evaluation and cognitive processing of decision (Gottfried, 2011; Yeshurun et al, 2009; Chu and Downes, 2000).

Like other cortical areas, the PC receives diffusely distributed inputs from cholinergic, noradrenergic, serotonergic, dopaminergic and histaminergic cells located in the basal forebrain, brainstem, and hypothalamus (Neville and Haberly, 2004).

4.3 Diseases affecting the olfactory system

Olfactory dysfunction is a cardinal symptom in several disease entities: It is globally impaired in idiopathic Parkinson's disease, Alzheimer's and Lewy body dementia, and multisystem atrophy (Herting et al., 2008; Wattendorf et al., 2010). It might be even a prodromal sign of Alzheimer's disease (Baba et al., 2012). In Schizophrenia no reliable change in odour sensitivity is reported, but deficits in odour identification, recognition and discrimination. In major depression hedonic aspects of odour perception and in some cases, alterations in sensitivity and identification were seen (Atanasova et al., 2008). Whereas olfactory function cannot serve to make the important differential diagnosis between Alzheimer's disease and geriatric depression, it might be useful to distinguish idiopathic parkinson's disease from progressive supranuclear palsy, essential tremor, vascular parkinson's disease or corticobasal degeneration (Liberini et al., 2000; Atanasova et al., 2008; Herting et al., 2008). Olfactory function seems to be disturbed very early in Alzheimer's and Parkinson's disease progression. In contrast to depression and schizophrenia, dysosmia and anosmia correspond to alterations specific to the OB and PC (Wattendorf et al., 2009; Li et al., 2010; Wesson et al., 2010). Another disease affecting specifically the PC and sourrounding regions is temoral lobe epilepsy (McIntyre and Gilby, 2008).

Understanding physiological information processing in the PC thus might help to understand early changes in disease processes.

4.4 Cell Type Specific Subcircuits – Hypothesis

From the network theory perspective, different elements of microcircuit organization underlie sensory and associative memory-related cortical processing: Afferent feed forward excitation in sensory microcircuits from relays like the thalamus (or OB) supports sensory (serial) processing. Recurrent feedback excitation in intracortical microcircuits mainly mediates associative memory-related processing in associative brain areas like the CA3 region of the hippocampus (parallel processing; Treves and Rolls, 1992; Douglas and Martin, 2010). These concepts underlie opposing theoretical network models of the PC: some authors describe a serial processing architecture (Ambros-Ingerson et al., 1990), others focus on features of parallel processing (Barkai et al., 1994). In vivo current source density analysis in the aPC revealed the sequential activation of sensory and intracortical synapses on aPC principal cells (Ketchum and Haberly, 1993). Therefore, more recently these concepts have been merged into the proposition of the anterior Piriform Cortex (aPC) as a 'hybrid recurrent/feed forward pattern correlation network' (Haberly, 2001). In our research, we aimed at assessing the role of these feedforward sensory and local corticocortical associative subcircuits in driving principle cells in the aPC.

Most current descriptions of PC sensory activation and local microcircuitry ignore the existence of different populations of excitatory cells in layer II and III. Mostly they put together superficial layer II and deep layer III pyramidal cells, do not mention semilunar cells at all and imply a convergence of sensory and associative inputs on the pyramidal neurons. However, Suzuki and Bekkers (2006) characterised superficial pyramidal cells and semilunar cells as two cell classes having distinct locations, input synaptic properties and output firing properties. For the six-layered neocortex it is known that the layering and physiological differentiation of principle cells corresponds to a functional specialisation: Ascending sensory and descending intracortical microcircuits are distributed

(however overlapping) to distinct cell populations in different layers. Sensory inputs from the thalamus mostly target on small layer IV granule pyramidal or stellate cells and to a lesser degree on layer III pyramidal neurons. Layer IV subsequently projects onto layer II/III, which shows extensive lateral connections and distributes intracortical associative fibers. These descending inputs terminate mostly in layer V/IV (Douglas and Martin, 2004; Shipp, 2007; De Felipe and Jones, 2010). In analogy, the differences in anatomical location and physiological characteristics of PC principle cells lead to the hypothesis that they exhibit a distinct integration into ascending sensory and local associative microcircuits and might thereby fulfil a different function.

In our study, we therefore aimed at a quantitative assessment of aPC functional microcircuit organization in acute slices of rat brains with respect to these two sensory and intracortical subcircuits and the role of the different cell types in these circuits. We used fast population two-photon Ca^{2+} imaging to probe LOT-mediated afferent sensory inputs to layer II and laser scanning photostimulation (LSPS) to quantify intracortical circuitry in layer II/III principal cells of the aPC (Wiegand et al., 2011).

5 METHODS

5.1 Experimental Procedures

5.1.1 Slice Preparation

Experiments followed approved national and institutional guidelines for animal use. Acute slices of the APC (400 µm thickness) were prepared from wistar rats of either sex (age: postnatal 18–25) in a coronal plane perpendicular to and containing the LOT (Fig. 2) (Johenning et al., 2009).

5.1.2 Electrophysiology

Whole-cell voltage and current-clamp recordings were performed with a Multiclamp 700B Amplifier (Molecular devices). Data were digitized (National Instruments BNC-2090, Austin, TX, USA) at 5 kHz, low-pass filtered at 2 kHz and recorded stimulation point-specific with Morgentau M1 microscope software (Morgentau Solutions, Munich, Germany) or Igor Pro (Wavemetrics, Lake Oswego, OR). For calibration experiments, patch electrodes (with electrode resistances ranging from 3 MΩ to 6 MΩ) were filled with (in mM): 135 K-gluconate, 20 KCl, 2 MgATP, 10 Hepes, 0.2 EGTA, 5 phosphocreatine, 0.2% Biocytin, pH 7.3. For mapping experiments, the intracellular solution consisted of (in mM): 150K-gluconate, 0.5 $MgCl_2$, 1.1 EGTA, 10 phosphocreatine, 0.2% Biocytin, pH 7.2. Cells were held in voltage clamp between –65 and –75 mV. Initial access resistances were below 25 MΩ after breakthrough and not allowed to vary more than

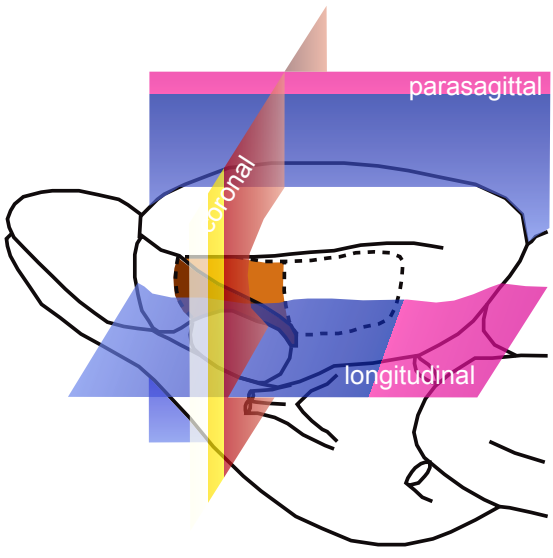

Figure 2 *– Slicing plane*
All experiments were done in acute aPC slices in a coronal slicing plane.
(modified from Demir et al., 2001)

30% during the course of the experiment in the voltage clamp mode. No access resistance compensation was used.

5.1.3 Glutamate uncaging and scanning of glutamate-evoked activity

Laser scanning photostimulation (LSPS) by glutamate uncaging and recording of the glutamate-evoked activity were performed on the setup described in Figure 3. For a detailed description see Bendels et al., 2008. In brief, the laser beam of a modified DPSS laser System (Rapp Optoelectronics, Wedel, Germany; DPSS Lasers, Santa Clara, CA, USA) with 355 nm wavelength, frequency-tripled Nd:YVO 4, 100 kHz pulse repetition rate) was delivered to a standard Olympus BX-51 WI microscope (Olympus, Hamburg, Germany) with a 200 µm fiber optic light guide coupled into the epifluorescence port of the microscope and focused on the specimen by the objective lens. The duration of the light stimulus was controlled by a fast galvanometric driven shutter system controlled via a computer-internal PCI-I/O card (Multifunction-Data-Aquisition NI-PCI-6221, Shielded Connector Block NIBNC-2110, National Instruments, Austin, TX, USA). The microscope optics and, hence, the laser spot was positioned by a motorized XYZ-shifting table with a stepsize of 0.1 µm (Shifting Table 380, Luigs & Neumann, Ratingen, Germany), so that the specimen and the recording electrode remained in a fixed position. For the optical control of the experiment a VX55 IR-camera (Till Photonics, Munich, Germany) generated an analog video signal, which was read out by a computer-internal frame-grabber card (DT-3120, Data Translation, Bietigheim Bissingen, Germany) and displayed in real-time. The communication software (on the operating system Windows) was hosted on a standard personal computer with a 1.2 GHz Pentium processor and 1 GB of RAM. For triggering of the laser stimulus, control of the XYZ-table, planning and execution of the experiment and data acquisition, we used the Morgentau M1 microscope software (Morgentau Solutions, Munich, Germany) (Bendels et al, 2008).

For the experiment, 20 ml of 200 µM 4-methoxy-7-nitroindolinyl-caged-l-glutamate (Tocris, Bristol, UK) were recirculated at 3–5 ml/min. The maximum time period of recirculation was 3 hours. The duration of the laser flash was 2 ms,

the laser power under the objective, corresponding to the stimulus intensity levels used, was calibrated (see 6.1.2 and 7.1) with a photodiode array-based photodetector (PDA-K-60, Rapp Optoelectronics, Wedel, Germany). The optical system was adapted to achieve an effective light spot diameter of 15 µm in the focal plane. Generally, stimulation points were defined in a hexagonal grid with a raster size of 30 µm. For all experiments, the focal depth of the uncaging spot was set at 50 µm below the slice surface. To correct for differences in focal depth of the uncaging spot due to variability in slice surface height, we adjusted the focal depth

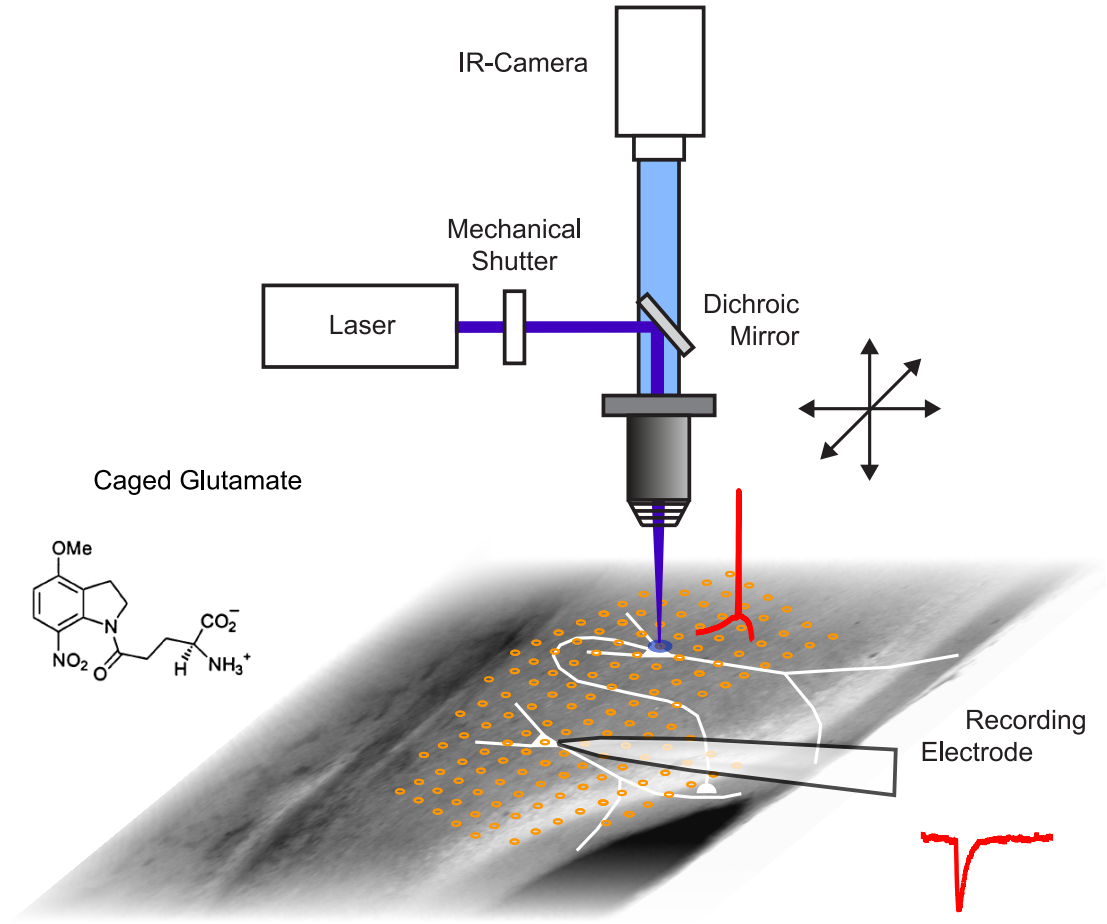

Figure 3 *– Laser scanning photostimulation setup*
Principle components light path and experiment configuration of the laser scanning photo stimulation setup. The Morgentau M1 software controls all components. The 2 ms laser light beam uncages at a defined location chemically inactivated glutamate. This drives nearby cells (if they are in the critical distance d*, see figure 4 and section 6.1.2) to spike. If the spiking cell is connected to the recorded cell, postsynaptic currents can be observed. By rastering the slice surface, a map of presynaptic input sites can be obtained.

different subregions (Fig. 10A and B, 11A and 12A and B). These subregions were scanned in a randomized order. It is known that MNI-caged-Glutamate influences inhibition (see Tocris product description of MNI caged L-Glutamate, Cat. Nr 1490, http://www.tocris.com/ dispprod.php?ItemId=22603). We therefore tested the effect of 200 µM MNI-caged-glutamate, the same concentration that we used in our mapping experiments, on stimulation evoked IPSCs in superficial pyramidal cells. Drug application was reducing IPSCs by about 30-50 % (Fig. 4). However, we were considering inhibition as relatively intact, as in our hands, blocking of inhibition with 2 µM of gabazine resulted in large depolarizing events (see Beed et al., 2010), that we did not see during our LSPS-Exeperiments with MNI-Glutamate.

5.1.4 Histological procedures

Slices with biocytin-filled cells were fixed in 0.1 mM phosphate buffer (pH 7.4) containing 4% paraformaldehyde, for 24–48 h. Staining and reconstruction were performed with two methods:

Either the filled neurons were visualized by incubating sections in avidin-biotin-conjugated horseradish peroxidase (ABC, Vector Laboratories, Ltd., UK) and reacted with diaminobenzidine and hydrogen peroxide. Sections were then dehydrated and embedded on glass slides. Reconstruction and morphological analysis of the biocytin-labeled neurons were made with an Olympus BX61WI (Olympus, Hamburg, Germany) attached to a computer system (Neurolucida;

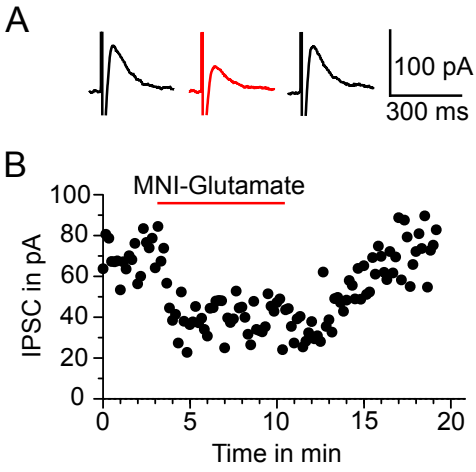

Figure 4 *– Inhibitory effect of MNI-Glutamate*
Effect of 200 µM MNI-Glutamate on stimulation evoked IPSCs in a L2P cell. The LOT was stimulated with a stimulation electrode with strength from 3.5 to 8 pA. IPSCs amplitudes were between 50 and 100 pA. Excitation was blocked with 50 µM APV and 10 µM NBQX.
A Example Traces: Black traces – baseline and after washout, red trace – presence of MNI-Glutamate.
B IPSC Amplitudes: baseline – 200 µM MNI-Glutamate – washout. 0.03 Hz stimulation frequency

Micro- brightfield Europe, Magdeburg, Germany) (Beed et al., 2010).
Alternatively, slices were incubated with Avidin-coupled Alexa 488 (Sigma-Aldrich, München) in phosphate buffer, washed in ethanol, embedded on glass slides with Fluoromount (Sigma-Aldrich, München). Images were taken with a laser-scanning confocal microscope and the pictures were processed with the open source image processing software ImageJ.
Data were not corrected for tissue shrinkage. The reconstructed cells were superimposed onto the photomicrograph of the native slice with standard graphics software.

5.1.5 Two-Photon Calcium Imaging (TPCI)

For fluometric Ca2+ measurements, we modified the multi-cell-bolus-loading procedure (Stosiek et al., 2003) adapted to slice preparations (Johenning and Holthoff, 2007). In brief, 200 µM of the red morphological marker CellTracker Red CMTPX were added to 1mM OG-BAPTA1-AM. Application was performed at three different locations (between layer I and II, in layer II and between layer II and III) at 100 mbar. The application pipette was inserted dorsally from the LOT and the imaged field of view (towards the perirhinal fissure) (Fig. 5B). The stimulation electrode was placed in layer 1a, ventrally between the LOT and the imaged field of view (i.e. towards the LOT). Intracortical inputs were selectively blocked by 30 µM baclofen (Tang and Hasselmo, 1994; Franks and Isaacson, 2005; Johenning et al., 2009). Stimulation strength was adjusted to be at the threshold for activation of at least one cell in the population with two consecutive stimuli.
Two-photon imaging was performed on a two-photon laser-scanning system (Femto2D, Femtonics Ltd., Budapest) equipped with a femtosecond laser tuned to 810 nm (Chameleon, Coherent). For epifluorescence, we used an Olympus XLUMPLFL 20x/0.95 N.A: water immersion objective, trans-fluorescence and transmitted IR were collected with an Olympus oil immersion condenser. A diagram of the light path is shown in Figure 5A (Chiovini et al., 2010). Multiple cells (20-30) within a field of view were scanned at constant speed (125 Hz or 250 Hz) (Fig. 5C, red path sections) while intermediate sections were jumped over within

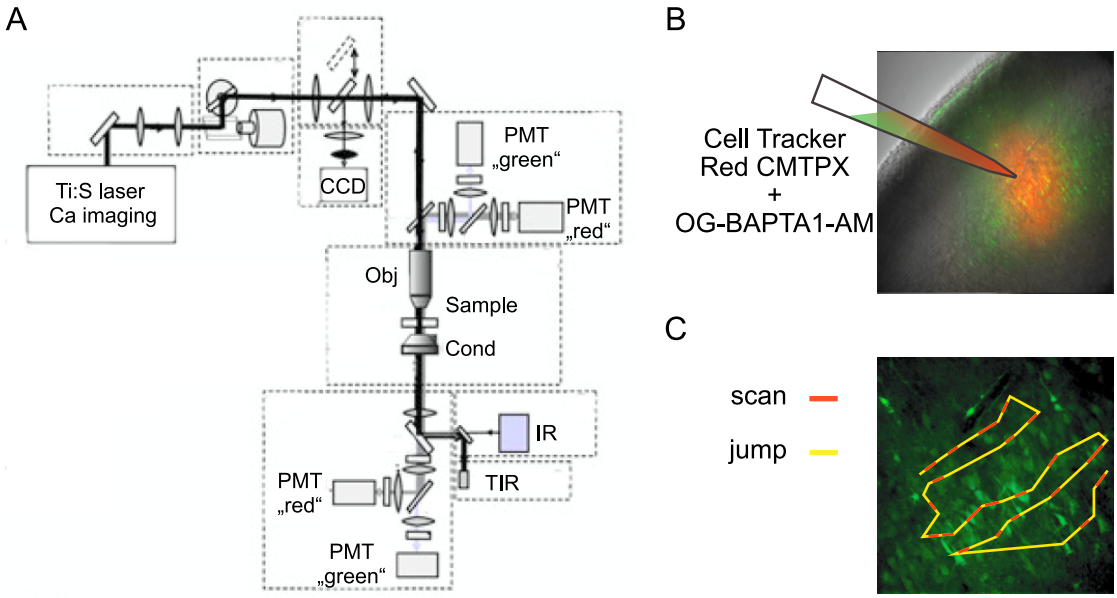

Figure 5 *– Two-photon population imaging setup.*
A Principle components and light path of the two-photon population imaging setup. Abbreviations: CCD – charge-coupled device camera; Cond – condensor; IR – infrared light source, Obj – objective; PMT – photomultiplier; TIR - transmission infra red detector (from Chiovini et al., 2010).
B Cell Tracker Red CMTPX as a red morphological marker and OG-BAPTA1-AM as a voltage sensitive dye are injected with 100 mbar into the slice. Sensory inputs are stimulated with a stimulation electrode positioned in layer Ia, intracortical inputs were selectively blocked by 30 µM baclofen.
C The calcium response of multiple cells is imaged using multiple line scanning. Only red parts of the indicated track are scanned, while the yellow intermediated sections are jumped over within 60s.

60 µs, using a spline-interpolated path (Multiple Line Scanning; Lorincz et al.,2007) (Fig. 5C, yellow path sections). Measurement control, data acquisition and analysis were performed using the Matlab-based MES program package (Femtonics Ltd., Budapest). Cells covered by the multiple line scan were blindly and randomly picked before stimulation.

5.2 Data analysis and statistics

For cell type classification, we used three parameters: input resistance, burst index and normalized depth for layer II cells. The burst index was calculated as $\Delta t_2/\Delta t_1$, where t_1 is the time interval between the first and second AP, and t_2 between the second and third AP, in a 600-ms-long train of eight APs (Suzuki and Bekkers,

2006). The superficial and deep border of layer II were defined on visual inspection of low-magnification DIC images. Cells were localized on a normalized vertical axis, with 0 being the superficial and 1 the deep border.

5.2.1 Analysis of LSPS data

For detection of synaptic events, we used the automatic detection method described by Bendels et al . 2008. The iterative algorithm is based on four criteria: the absolute peak amplitude (larger than 10 pA), the maximum absolute slope of the rising part of the PSC (faster than 2.8 pA/ms), the time-interval between the initiation of the PSC and its peak (shorter than 13 ms) and the total amount of electric charge that is transported out of the cell (negative for EPSCs and positive for IPSCs) (Bendels et al., 2008). Parameters used by the algorithm were based on visual inspection of the raw data. Inputs were classified as direct if they occurred in the first 5 ms after the light beam. This distinction between direct and indirect inputs was verified recently by the analysis of the temporal occurance of current clamp responses and by TTX control experiments (Bendels et al., 2010). Fig. 7B displays examples traces with events detected by the algorithm. The IPSC information was not analysed in this study.

In a second analysis step, a second algorithm was used for discriminating photoactivated synaptic inputs (synaptic points) from random background activity. It is based on the observation that a presynaptic cell has several neighbouring activation sites (Fig. 8A, B and C; 10B and C). Consequently, spatial correlation of inputs indicates specific activation. To extract significant spatial correlations, we tested the significance of the number of observed inputs in a restricted region against the null hypothesis of a random spatially uncorrelated pattern. A detailed description of this algorithm is given in Bendels et al., 2010.

To work out spatial differences in connectivity between the different cell populations, we defined a layer-specific connectivity coefficient, calculated as the ratio of positive synaptic points to all scanning points in a layer (synaptic $\text{points}_{\text{layer}}$/$\text{scanning points}_{\text{layer}}$).

For analyzing differences of input positions in relation to the dorsoventral main

axis, we distinguished layer-specific dorsal and ventral sectors by constructing an axis through the cell body perpendicular to the surface or the aPCX layer I/LOT border. We observed a wide and patchy distribution of inputs (see, for example, Fig. 10A, B and 12A). For each individual cell, we aimed at finding a measure of how the inputs are distributed on both sides of the axis. The first step was to calculate the sector-specific connectivity coefficient analogous to the layer specific connectivity coefficient (synaptic $points_{sector}$/scanning $points_{sector}$), in which a sector is defined as the stimulated area on one side of the axis. A comparison of the relative weight of inputs on either side of the axis between different cells needs to be independent of the baseline connectivity. It was therefore necessary to correct for differences in overall connectivity. The correction factor for a cells's overall connectivity was determined as the quotient of scanning $points_{TOTAL}$ and synaptic $points_{TOTAL}$. When calculating the position coefficient of a given sector for a given cell (synaptic $points_{SECTOR}$/scanning $points_{SECTOR}$)*(scanning $points_{TOTAL}$ /synaptic $points_{TOTAL}$), cells with large overall connectivity will have a small correction factor and cells with small overall connectivity will have a large correction factor. We then subtracted the ventral from the dorsal position coefficient for each layer in every cell. Values >0 indicate an asymmetry towards the dorsal side, values <0 an asymmetry towards the ventral side.

5.2.2 Analysis of Population Calcium Imaging Data

For analysis of population Ca^{2+} imaging data, fluorescence traces are expressed as relative changes in fluorescence ($\Delta F/F=(F-F0)/F0$), with F0 being the averaged prestimulus fluorescence. Traces from 5 consecutive experiments were averaged. For comparison with the 125 Hz data, two consecutive frames were averaged in the data acquired with 250 Hz, which leads to an effective sample rate of 125 Hz. We determined the onset sweep number (at 125 Hz scanning speed, each 8ms line cycle represents one sweep) of each individual cell's somatic Ca^{2+} transient: For determination of the signal onset, the standard deviation of the baseline signal was calculated. The line scan data was binned in 8 ms sweeps based on the 125 Hz sampling frequency in order to compensate for differences in acquisition time

points between subsequent pixels in a scanned line. The onset was defined as the first sweep where the amplitude was larger than 2 x SD of the baseline (SD_b). To qualify as an onset signal, this increase had to be followed by at least 5 sweeps with peak amplitudes larger than 2 x SD_b interrupted by a maximum of 6 sweeps with peak maxima below 2xSD_b. These criteria were verified in control experiments: Single APs were evoked by synaptic stimulation and recorded in cell-attached mode. The accompanying Ca^{2+} transient were measured in bolus-loaded layer II cells using image acquisition conditions similar to the ones used for collecting the population data. The single-AP induced Ca^{2+} transients were clearly identified by the proposed detection criteria in 5 out of 5 cells from independently stained slices (Fig. 13A). Cells were excluded as compromised cells if there was a constant rise of the fluorescence signal for 200ms post-stimulus. Selection of cells for line scanning was done blindly before the first stimulus was given. Layer II was subdivided into cell rows blindly before analysis. Cells from each experiment were dichotomized into a superficial (superficial half of rows in an experiment) and a deep (deep half of rows in an experiment) group. If there was an uneven number of rows, the row in the middle was not analysed (Fig. 13B).

5.2.3 Statistics

Statistical tests were performed using a two-tailed Mann-Whitney-U test and Kruskal-Wallis test with Dunn's Multiple Comparison as a posthoc test (referred to as Kruskal-Wallis test) as appropriate. Testing of correlations was based on Pearson's correlations. Numerical values are given as mean ± SEM. The detection of synaptic events, the calibration analysis and the cluster-analysis were performed using Matlab (The Mathworks, Natick, MA), all other statistical and graphical analysis with Microsoft Excel (Microsoft Cooperation, Redmond, WA), Graphpad Prism (Graphpad Software, San Diego, CA) and ImageJ, the figures were made with Adobe Illustrator CS5 and Adobe Photoshop Elements (Adobe Systems, San Jose, CA).

6 RESULTS

6.1 Cell Types and Calibration

6.1.1 Principle Cell Types in the Piriform Cortex

Based on different projection patterns, the compact layer II has been subdivided into a superficial layer IIA and a deep layer IIB (Haberly and Price, 1978, Fig. 1C). Within layer II, there is a functional and morphological diversity of different principal cells. At the extreme, pyramidal cells deep in layer II (L2Ps) have been morphologically (Haberly, 1983), biophysically (Suzuki and Bekkers, 2006; Suzuki and Bekkers, 2011) and functionally (Suzuki and Bekkers, 2011) distinguished from semilunar cells (L2Ss) that are located more superficially. In contrast to this apparent dichotomy, a graded morphological transition from semilunar cells to superficial pyramidal cells in layer II has been described, yielding semilunar-pyramidal transition cells (Yang et al., 2004) (Fig. 6B and C). Superficial pyramidal cells in layer II (Fig. 6D) are gradually replaced by layer III pyramidal cells (L3Ps) constituting the main population of principal neurons in superficial layer III (Fig. 6E). In deep layer III and endopiriform nucleus, multipolar cells (L3Ms) dominate as the main principal cell type (Neville and Haberly, 2004, Fig. 4F).

Different principal cell types in the aPC were distinguished based on characteristic biophysical properties (Suzuki and Bekkers, 2006), vertical position, and morphology (Haberly, 1983; Yang et al., 2004), although the latter was only taken into account when probing the excitability of cells upon laser stimulation for calibration. We analysed excitatory cells distributed over the whole vertical axis of layer II (Fig. 6A to D). When plotting input resistance against normalized position on the vertical axis of layer II, we observed a linearly correlated transition from superficial cells with high input resistance to deep cells with low input resistance

Figure 6 *– Biocytin reconstructions and input-output-curves demonstrating the vertical transition*
A a 'canonical' semilunar cell (cluster L2S), ***B*** a semilunar-pyramidal transition cell (cluster L2S), ***C*** a superficial pyramidal cell (cluster L2P), ***D*** a superficial to deep pyramidal transition cell (cluster L2P), ***E*** a deep pyramidal cell (L3P).
F Biocytin reconstruction and Input-Output-Curve of a multipolar cell used for calibration (L3M).

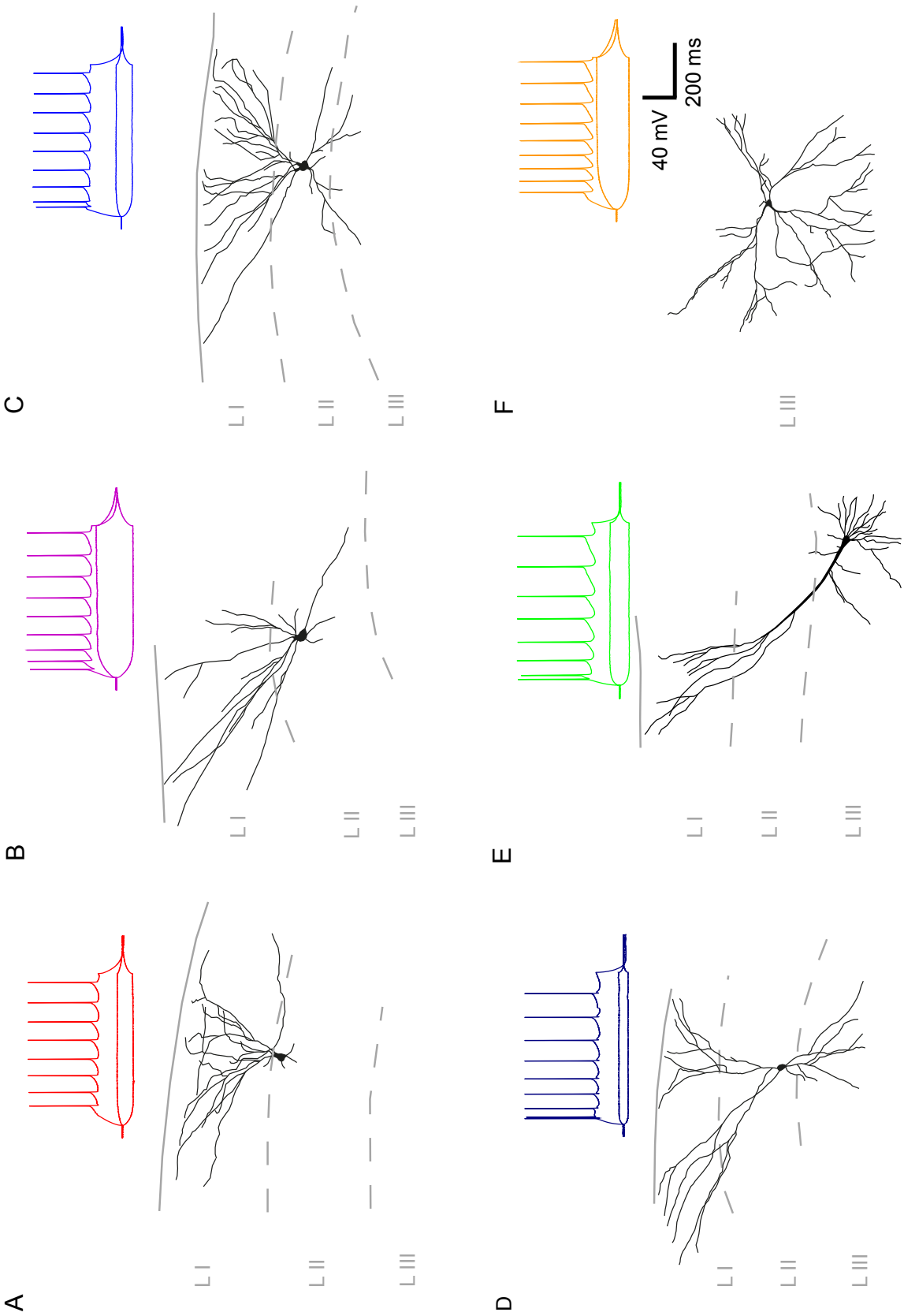
A
B
C
D
E
F
40 mV
200 ms

(Figure 7A, r=-0.67, p<0.001, n=64, see Materials and Methods for details). The burst index (indicating a cell's rate of spike frequency adaptation; see Materials and Methods) was also correlated with the input resistance in layer II cells (colour coding in Figure 7A, r=-0.44, p<0.001, n=64). High burst indices (i.e. a high rate of spike frequency adaptation correlated with an initial high-frequency burst) occur in deep cells with low input resistance and low burst indices occur in superficial cells with high input resistance.

To facilitate subsequent statistical analysis of local intracortical microcircuitry in superficial and deep cells of layer II, cells in this semilunar- to pyramidal-like transition were clustered into two groups. Taking into account three parameters input resistance, burst index and normalized vertical depth in layer II, we grouped the cells by a k-means cluster analysis (repeated with 100 different initial conditions). Based on these three parameters, we distinguished two clusters, that we called in analogy to their reference cell type L2S and L2P cluster (Fig. 7A). Within those clusters, we observed highly significant differences between L2Ss and L2Ps for all three parameters (input resistance: p<0.001; burst index: p<0.001; position: p<0.001; Kruskal-Wallis-test, Fig. 7B), despite the fact that they are overlapping in all three dimensions.

We note that here cluster analysis was merely used to generate groups for statistical comparison of intracortical connectivity. Although clustering (necessarily) assumes discrete cell populations, it is important to stress that our data cannot be interpreted to validate (nor to disprove) the existence of the two distinct cell clusters established by Suzuki and Bekkers (2011) using a much larger number of phenotypical indicators. Alternatively, gradients observed in our data would also be compatible with a continuous transition from a semilunar to a superficial pyramidal like phenotype within layer II (see 7.2).

In layer III, we could morphologically differentiate L3Ps and L3Ms: L3Ps have an early onset of AP firing upon depolarization, an initial burst when firing more than 2 APs (high burst index i.e. a high rate of spike frequency adaptation), a low input resistance and are found in superficial layer III. Multipolar cells demonstrate a long latency of AP firing upon depolarization, a regular firing pattern, a low input resistance similar to L3P and they are found in deep layer III (Figure 6F).

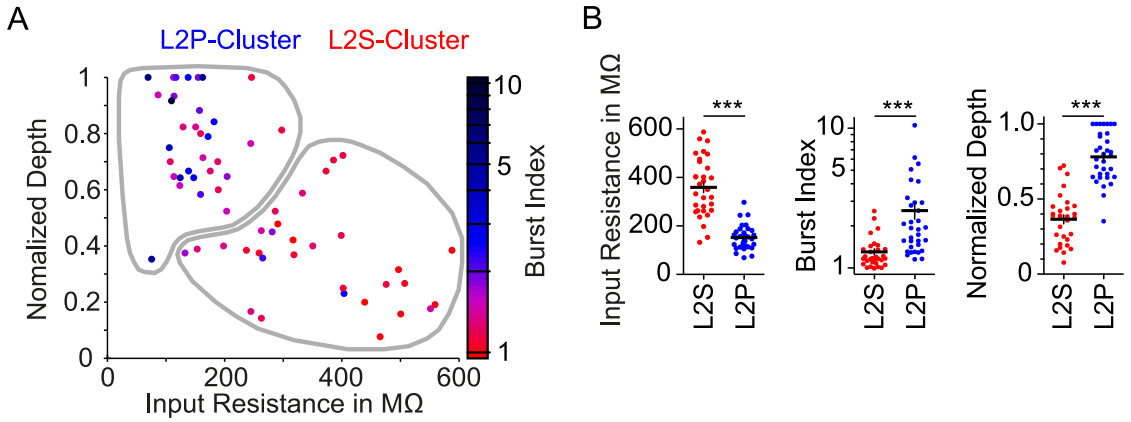

Figure 7 *– APC principal cells are organized in a continuous gradient*
A Plot of input resistance versus depth in layer II of the aPC. Colour code refers to burst index: Red indicates low spike frequency adaptation, blue high spike frequency adaptation. Within layer II, a functional and morphological diversity of different principal cells can be identified. Grey lines indicate populations defined for statistical comparisons between superficial and deep cells using a k-means cluster algorithm. In layer II, we distinguish two clusters for analysis: L2S containing more semilunar-like cells and L2P with more pyramidal-like cells.
B Comparison of the two clusters for the parameters underlying the analysis yields significant differences.

6.1.2 Calibration of Spatial Resolution

We next wanted to compare the layer-specific intracortical connectivity patterns between L2Ss, L2Ps and L3Ps using LSPS. Focal photolysis of caged glutamate by LSPS induces direct and indirect synaptic responses in the recorded neuron (called target cell). The direct responses are evoked by glutamate uncaged close to the somatodendritic compartment of the recorded target cell. Indirect synaptic responses reflect suprathreshold direct activation, i.e., action potential (AP) firing of a presynaptic neuron projecting onto the recorded neuron (called source cell). We first determined the laser intensity that permits maximal spatial resolution. A measure of spatial resolution for LSPS is the critical distance d*, which is the distance from the putative source cell's soma where 75% of all cumulated APs could be evoked as direct responses. The distance d* depends on cell type and laser intensity. It estimates the distance between cell soma and dendritic hotspots, i.e., the location on the dendritic arbour from which an AP is evoked by photolysis of

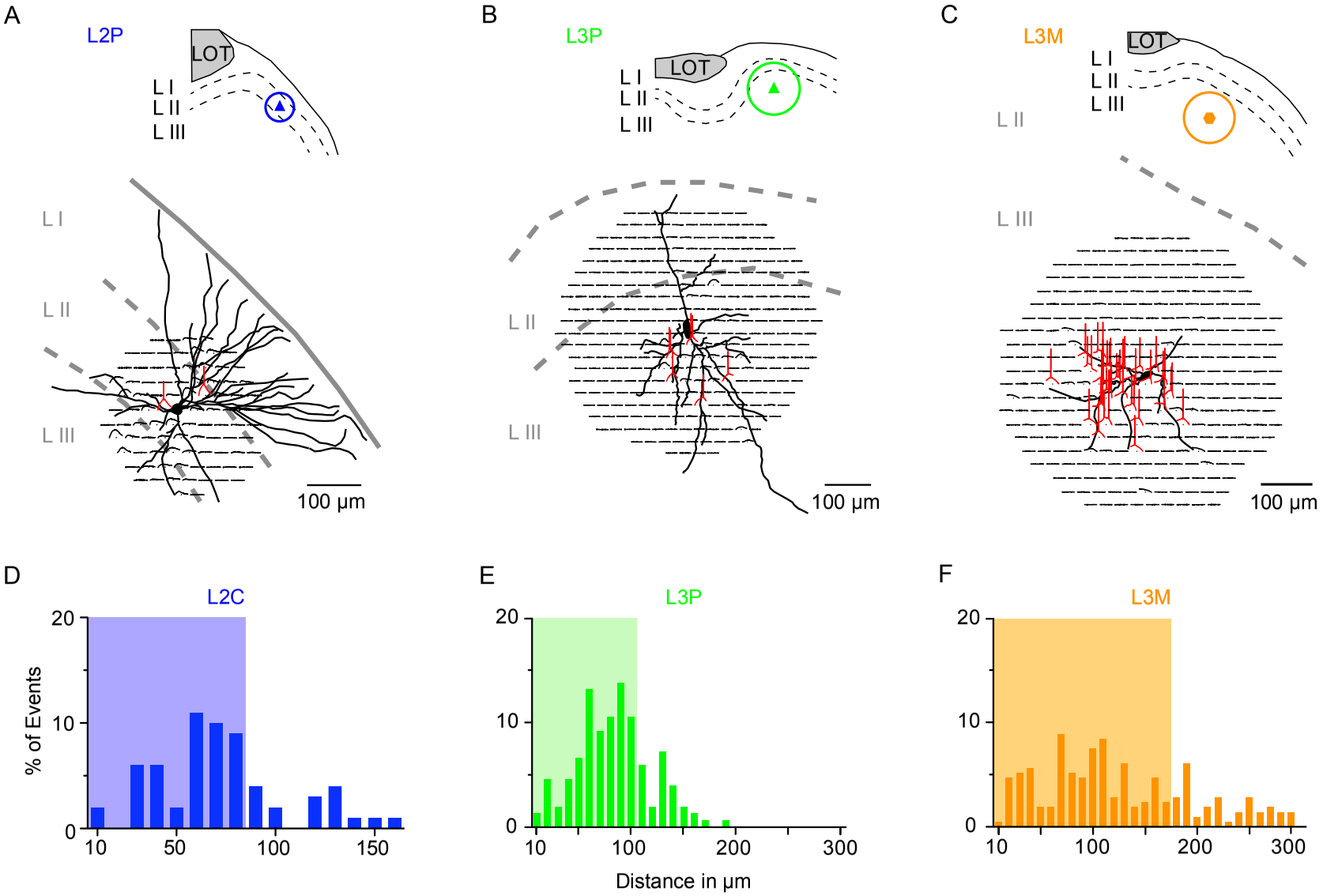
A
L2P
LOT
L I
L II
L III
100 µm
B
L3P
LOT
L I
L II
L III
100 µm
C
L3M
LOT
L I
L II
L III
100 µm
D
L2C
% of Events
20
10
0
10
50
100
150
E
L3P
20
10
0
10
100
200
300
Distance in µm
F
L3M
20
10
0
10
100
200
300

Figure 8 *– Resolution of photoactivation by glutamate uncaging*
A-C Sketches on top mark the position of three example principal cells within the aPC coronal slice. Below, biocytin reconstructions are overlaid with direct inputs evoked by LSPS measured in current clamp. Perisomatic suprathreshold activation is demonstrated by red APs. The stimulation pattern consisted of points with 30 µm spacing. Spatial profiles of excitability of the main aPC excitatory cells were performed at different laser intensities. ***A*** Layer II pyramidal cell (L2P, blue) to represent layer II cells (L2C, see D), ***B*** layer III pyramidal cell (L3P, green), ***C*** multipolar cell (L3M, orange).
D-F Distribution histograms of suprathreshold activation as a function of the distance from the calibrated cells' somata. APs were counted in 10 µm spatial bins. Shaded boxes correspond to d*, where 75% of all inputs were observed. L2Ps and L2Ss grouped as L2Cs, (n=26), 83.5 µm; L3 pyramidal cell (L3P, n=6) 97.2 µm; multipolar cell (L3M, n=9), 170.7 µm.

caged-glutamate (Shepherd et al., 2003; Bendels et al., 2008; Beed et al., 2010). We generated spatial profiles of AP firing of the main excitatory cells in all layers of the aPC in current clamp. We scanned a radius of 150 µm for the superficial cells (Fig. 8A) or 300 µm for the deep cells (Fig. 8B and C). The scanning pattern consisted of points with 30µm spacing. In Fig. 2, we overlaid camera lucida reconstructions of representative cells with subthreshold (black) and suprathreshold (red) direct responses elicited at each scanning point. We observed perisomatic clustering of action potentials (APs, Fig. 8A, B and C). Fig. 8D, E and F display the fraction of APs depending on the distance from the cell soma for each cell type at the laser intensity used for our experiments. Calibration was performed for a wide range of laser intensities, and the laser intensity yielding the best resolution was used throughout the mapping experiments. The resulting cell-type–specific d* values at the laser intensity used for our subsequent mapping experiments were as follows: L2 principal cells (L2Ps and L2Ss grouped as L2Cs, n=26), 83.5 µm; L3 pyramidal cell (L3P, n=6) 97.2 µm; multipolar cell (L3M, n=9), 170.7 µm (Fig. 8D, E and F).

6.2 Probing associative inputs by LSPS

6.2.1 Generation of principal cell-type specific afferent input maps from different APC layers

For interpretation of afferent maps, we first had to define the time interval after the uncaging flash used for collecting indirect monosynaptic inputs. Synaptic inputs were collected up to 100 ms following UV photolysis (light blue boxes around the example traces in Fig. 9A, B and 10C). Representative traces of the time

course of APs evoked by direct stimulation in calibration experiments are displayed in Fig. 9A. The bursting behaviour of superficial cells and the long membrane time constant of deep layer principal cells (Tseng and Haberly, 1989) explain temporal delays in the range of 100 ms after the uncaging flash (see Fig. 9D for a quantification of temporal delays to first and last APs as evoked by uncaging). This is reflected by the increase of PSC rates in this time frame (Fig. 9C).

Polysynaptic activation would result in degradation of spatial resolution of our data. We therefore analysed our calibration data to see if indirect inputs evoke suprathreshold postsynaptic responses resulting in AP firing. In L2Ps and L2Ss, APs within our 100 ms analysis window were always elicited by direct activation of the recorded cells (100%, average of 26 cells). In L3Ps (n= 6 cells), the average probability of indirectly activated suprathreshold responses was 2.2 ± 1 % per cell. In L3Ms (n=9 cells), this average probability value was 3.8 ± 6 %. We therefore consider uncaging-induced synaptic inputs to be largely monosynaptic.

We separated the direct and indirect synaptic responses by their different delay-to-onset times. Direct responses were elicited almost immediately in a time window of 10 ms after the UV flash (flash indicated as dark blue stripe in example traces in Fig. 5A, B and G; see also Materials and Methods). Indirect activation can be extracted on top of direct activation (Fig. 9B, trace 2), enabling us to also define local synaptic points. All inward currents are defined as EPSCs and could be clearly distinguished from inhibitory outward currents (Fig. 9B, traces 3 and 4).

The synaptic responses collected in the specified time interval contain specific photo-induced synaptic inputs and unspecific spontaneous activity. The next step was the distinction between such photo-evoked and spontaneous responses. For discrimination between specific synaptic inputs and background activity, we used a spatial-correlation–based algorithm to extract presynaptic input locations (see Materials and Methods; Bendels et al., 2010; Beed et al., 2010). Scanning points corresponding to photoactivation-induced inputs were termed synaptic points, and afferent maps were constructed based on these synaptic points (red points in Fig. 10A (L2S), blue points in Fig. 10B (L2P), green points in Fig. 12A (L3P)).

Input from distinct layers was compared for different principal cells: Mapping of local intracortical synaptic inputs was performed for L2Ss, L2Ps and L3Ps. For

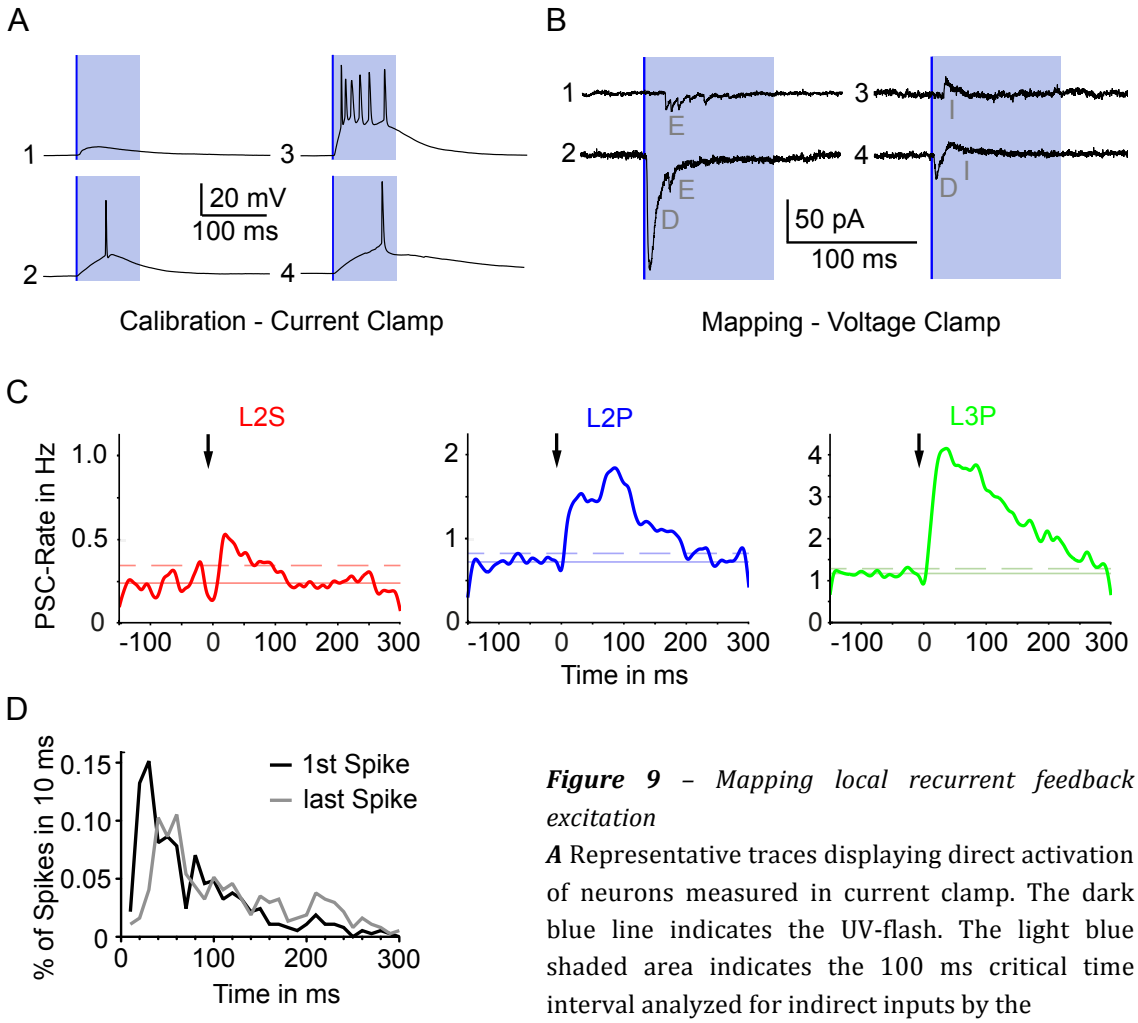

Figure 9 *– Mapping local recurrent feedback excitation*

A Representative traces displaying direct activation of neurons measured in current clamp. The dark blue line indicates the UV-flash. The light blue shaded area indicates the 100 ms critical time interval analyzed for indirect inputs by the detection algorithm.

B Representative traces displaying the different classes of events in voltage clamp detected by the analysis algorithm. Indirect excitatory response: E; Direct excitatory response: D, indirect inhibitory response: I.

C Averaged postsynaptic current (PSC) incidence rates for L2S (red), L2P (blue) and L3P (green) plotted over time. The arrow indicates the time point of photostimulation. A significant photostimulation-related increase can be observed in all cell types.

D Frequency distribution histogram of the latency of the first and last AP after the UV flash in 10 ms bins (370 traces with APs from 27 cells).

mapping, a hexagonal grid with a point-to-point distance of 30 µm was projected across the different layers (Fig. 10A, B and C, Fig. 12A). For analysis, the scanning region was grouped into the following aPC cortical layers: layer II (based on the spatial resolution calculated from our calibration data, we did not subdivide layer II into a deep and superficial layer for the source-cell analysis), superficial layer III (first 300 µm parallel to the layer II-layer III border) and deep layer III (below superficial layer III; Fig. 10A and B, Fig. 12A).

6.2.2 L2S, L2Ps and L3Ps: comparison of intracortical connectivity

For statistical comparison, target cells were classified as follows: Layer II cells were grouped according to the afore mentioned cluster analysis (superficial layer II 'semilunar phenotype' L2Ss vs. deep layer II 'pyramidal phenotype' L2Ps; Fig. 5A). L3Ps were identified as indicated above.

Due to anatomical variances between acute brain slice preparations, the number of scanning points per layer sampled in individual experiments differs. To compare connectivity between different cell types (i.e. across slices and experiments), it was necessary to normalize the number of detected synaptic points per layer to the total number of scanned points in this layer. For this purpose, we calculated layer-specific connectivity coefficients for each cell ($\text{synaptic points}_{\text{layer}}/\text{scanning points}_{\text{layer}}$; Fig. 8A, B and 10A). Target cell-type specific microcircuitry organization of the aPC can be evaluated by comparing layer-specific connectivity coefficients between cell types. A large connectivity coefficient indicates strong intracortical connections to a recorded target neuron from a given stimulated layer.

Layer II is the cell layer containing most of the aPC principal cells (Neville and Haberly, 2004). From layer II we observe a significantly higher connectivity coefficient in L2Ps (n=13) and L3Ps (n=15) compared to L2Ss (n=19; L2P vs. L2S: $p < 0.001$, L3P vs. L2S: $p < 0.05$; Fig. 9A).

L3Ps received significantly more inputs from deep and superficial layer III than L2Ss (superficial layer III L3P (n=14) vs. L2S: $p<0.01$, deep layer III L3P (n=17) vs. L2S: $p<0.01$; Fig. 6A). Comparing L2Ps to L2Ss, the intracortical connectivity from superficial and deep layer III was not significantly different (superficial layer III inputs: L2P (n=13) vs. L2S (n=15): n.s.; deep layer III inputs: L2P (n=14) vs. L2S (n=15): n.s.; Fig. 9A).

Next, we compared intracortical connectivity between L3Ps and L2Ps. For stimulation sites in layer II and superficial layer III, the average recurrent feedback connectivity of L2Ps was not significantly different from L3Ps (Fig. 11A). For stimulation sites in deep layer III, we observed a significantly higher connectivity coefficient for L3Ps than for L2Ps ($p<0.01$, Kruskal-Wallis test used for all

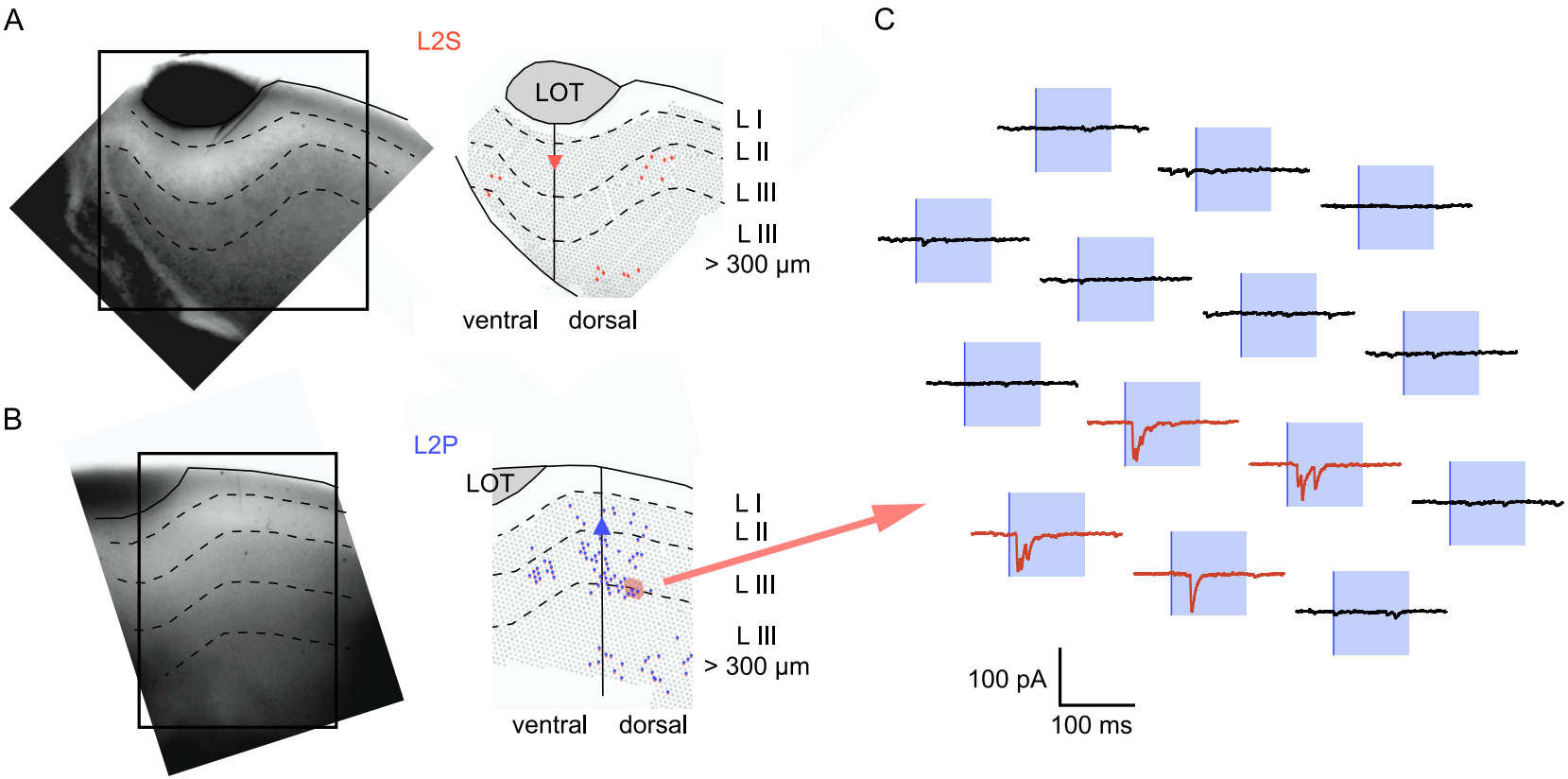

Figure 10 *– L2S and L2P example maps*

A Example map of an L2S (red triangle, target cell). ***B*** Example map of an L2P (blue triangle, target cell). Left, Low-magnification DIC images of the aPC coronal slice. Right, Corresponding scanning rasters and target cells are projected on the schematic drawings of the DIC images. Colored points indicate positive synaptic points detected as inputs from source cells. L I, layer I (not mapped); L II, layer II; L III 300 m, the first 300 μm of layer III parallel to the layer II/layer III border; L III 300 m, the part of layer III below 300 μm. The raster consisted of stimulation points separated by 30 μm.

C Example traces from the stimulation raster (red in B): 200 ms around the UV flash (indicated by dark blue line) are plotted. The light blue shaded area indicates the 100 ms critical time interval analyzed for indirect inputs by the detection algorithm. Traces positive for intracortical inputs are plotted in red, and negative traces are plotted in black.

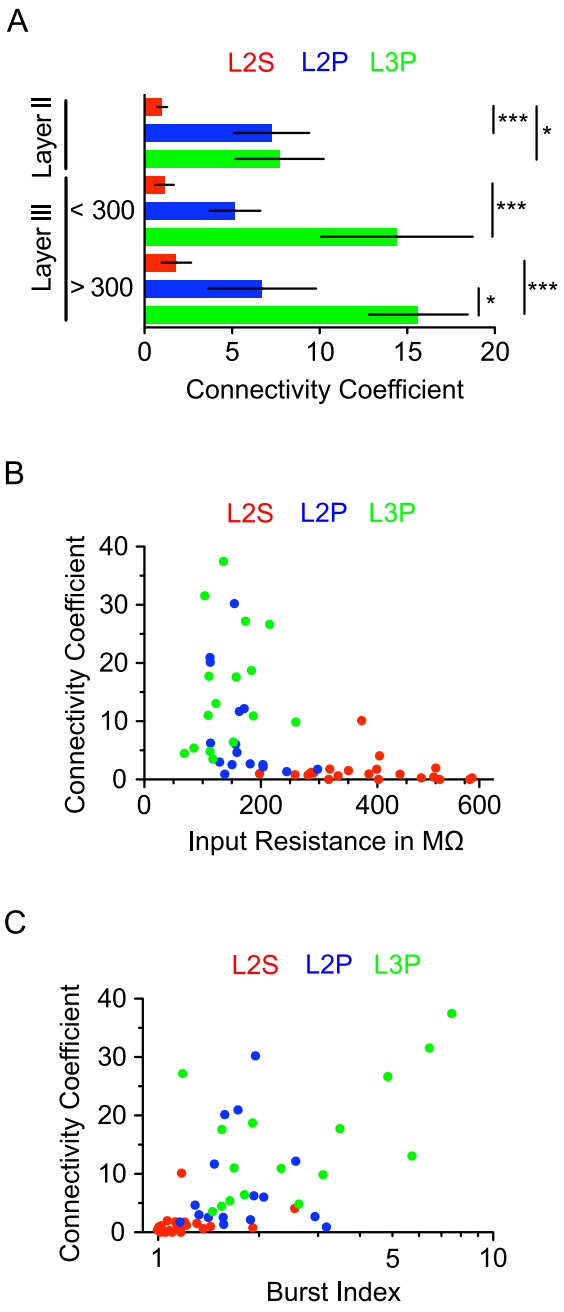

Figure 11 *– Intracortical connectivity increases from superficial to deep*

A Statistical comparison of the connectivity Coefficient of L2S, L2P (as distinguished by the cluster analysis) and L3P:

From layer II, L2Ps (7.3±2.2, n=13) and L3Ps (7.7±2.5, n=15) display a significantly higher connectivity coefficient than L2Ss (1.0±0.3, n=19; L2P vs. L2S: $p < 0.001$, L3P vs. L2S: $p < 0.05$). Compared to L2Ss, L2Ps do not display significantly larger intracortical connectivity from superficial layer III (L2P=5.2±1.4, n=13, L2S=1.2±0.5, n=15; L2P vs. L2S) and from deep layer III (L2P=6.7±3.1, n=14; L2S=1.8±0.8, n=15; L2P vs. L2S).

From both superficial and deep layer III, L3Ps were significantly higher connected than L2Ss (superficial layer III: L3Ps=14.4±4.3, n=14, L2Ps=deep layer III: 15.6±2.8, n=17; superficial layer III L3P vs. L2S: $p<0.01$, deep layer III L3P vs. L2S: $p<0.01$).

From layer II and superficial layer III, the average intracortical connectivity of L2Ps was not significantly different as compared to L3Ps (layer II: L2P=7.3±2.2, L3P=7.7±2.5; $p>0.05$; layer III: L2P=5.2±1.4, L3P=14.4±4.3; L2Ps vs. L3Ps: $p>0.05$). From deep layer III, we observed significantly higher connectivity index for L3Ps than for L2Ps (L2P=6.7±3, L3P=15.6±2.8; $p<0.01$, Kruskal-Wallis-test used for all comparisons).

B Overall connectivity from all layers correlates with the target cell's input resistance ($r=-0.49$, $p<0.001$, n=53).

C Overall connectivity from all layers correlates with the target cell's burst index ($r=0.66$, $p<0.001$, n=53).

comparisons in Fig. 11A). In sum, based on the groups of principal cells defined by clustering in layer II, we observe a superficial- to deep increase in the strength of an aPC principal cell's intracortical connectivity with respect to the target cell's position on the vertical axis (L2S<L2P<L3P).

We then plotted the input resistance (as a parameter indicative for a more L2S- or a more L2P/L3P like phenotype) of the mapped cells against their connectivity coefficient. Overall intracortical connectivity from all cortical layers clearly depended on input resistance: low input resistances were associated with highly connected cells (Fig. 11B, $r=-0.49$, $p<0.001$, $n=53$). We found a similar relationship between L2Ss, L2Ps and L3Ps when plotting the overall intracortical connectivity against burst index (Fig. 11C, $r=0.66$, $p<0.001$, $n=53$). The distribution of data points in these correlation plots suggests scaling of functional microcircuit incorporation with the intrinsic cellular properties input resistance and spike frequency adaptation along the superficial-to deep axis.

6.2.3 Layer III pyramidal cells: dorsal-ventral asymmetry of recurrent feedback excitation

So far, we quantified a given cell's incorporation into the local intracortical microcircuitry. We next asked whether the inputs were distributed symmetrically on the dorsoventral axis preserved in our coronal slicing plane. To analyse symmetry on the dorsoventral axis, we constructed each cell's main axis (the axis perpendicular to the layer I surface/LOT border that intersected the cell body, see also Beed et al., 2010) to divide the inputs into a ventral and a dorsal sector (Fig. 10A, B and Fig. 12A). In order to prevent the overrepresentation of cells with a high connectivity coefficient in our analysis, we corrected for a given cell's overall connectivity, resulting in a layer and sector specific position coefficient (for details, see Materials and Methods). This way, we could directly compare the relative weight of synaptic inputs from the dorsal and ventral sector as defined by the main axis between cells. For measuring differences between cell types, we calculated the layer- specific difference Δ between the dorsal and ventral sector's position coefficient (Δ=position coefficient$_{DORSAL}$-position coefficient$_{VENTRAL}$). Analyzing inputs from layer II ($n=14$) and deep layer III, onto L2Ps, we found almost symmetric connectivities in the dorsal and the ventral sector relative to the main axis ($n=12$; $p> 0.05$ for deep layer III vs. layer II inputs onto L2Ps, Mann-Whitney-U-test; Fig. 10C). The L3Ps revealed an asymmetric spatial shift of their deep layer

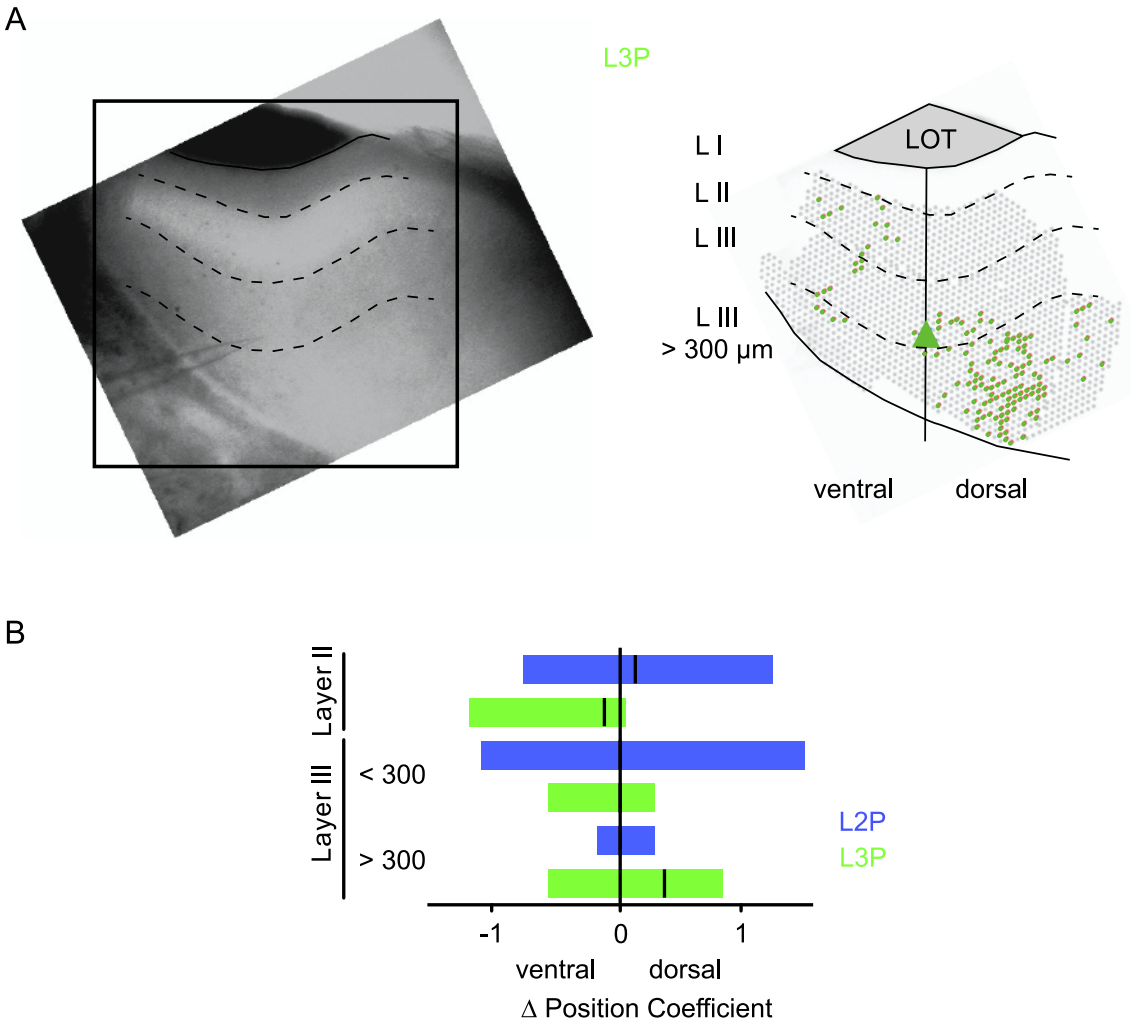

Figure 12 – *L3Ps receive asymmetric inputs on the ventrodorsal axis*
A Left, DIC image of the aPC superimposed with the layering used for analysis. Right, scanning raster and layering in the same magnification, positive synaptic points indicative of source cell activation are coloured in green, target cell is depicted by green triangle.
B Median (black lines) and 75 % percentiles of the position coefficient Δ are plotted for layer II, superficial III and deep III for L2Ps (blue) and L3Ps (green). L2Ps show symmetrically distributed intracortical inputs (layer II median Δ=0.12, n=14; superficial layer III Δ=0, n=13; deep layer III Δ=0, n=12; p> 0.05 for deep layer III vs. layer II inputs onto L2Ps, Mann-Whitney U Test). L3Ps have a clearly asymmetric position shift of their deep inputs towards the dorsal orientation (layer II median Δ=-0.12, n=14; superficial layer III Δ=0, n=16; deep layer III median Δ=-0.34, n=18; p< 0.05 for deep layer III vs. layer II inputs onto L3Ps, Mann-Whitney U Test).

III inputs (n=18) towards the dorsal direction when compared to layer II inputs (n=14) on the same cell type (p< 0.05 for deep layer III vs. layer II inputs onto L3Ps, Mann-Whitney-U-test, Fig. 10C). In sum, deep layer III intracortical inputs to L3Ps reveal an asymmetric organization along the dorsoventral axis.

6.3 Analysis of sensory input by fast TPCI reveals stronger recruitment of superficial layer II cells.

Using current source density analysis in vivo, sensory synaptic activation has been demonstrated to precede intracortical synaptic activity in the aPC (Ketchum and Haberly, 1993). We pharmacologically isolated this early, sensory component of aPC processing by selectively blocking associative fibers with baclofen (Tang and Hasselmo, 1994; Franks and Isaacson, 2005; Johenning et al., 2009). To compare the relative weight of sensory afferents within simultaneously stimulated populations of superficial and deep cells in aPC layer II, we used the multiple line scan technique (Lorincz et al., 2007) for fast two-photon fast population Ca^{2+} imaging (TPCI). Somatic Ca^{2+} transients evoked by synaptic stimulation indicate AP firing and scale with synaptic input strength (Smetters et al., 1999; Johenning and Holthoff, 2007; Dunfield and Haas, 2009, 2010). We first confirmed that our imaging approach faithfully reports single APs. We combined cell-attached recordings of layer II cells bolus-loaded with OG-1-AM with Ca^{2+} imaging. We were able to detect single-AP mediated Ca^{2+} signals in 5 out of 5 cells from 5 independently loaded brain slices (Fig. 13A). Multiple line scanning thus enables us to measure single-AP mediated somatic Ca^{2+} transients and superficial layer II cells simultaneously at a temporal resolution of 125 Hz.

On the level of the aPC network, the timing of a cell's AP output in relation to the other cells is the critical factor: In vivo, global inhibition in the aPC permits only for small windows of opportunity for AP-firing (Poo and Isaacson, 2009). Cells reaching the AP threshold too late will be silenced by inhibitory connections (Luna and Schoppa, 2008; Poo and Isaacson, 2009; Stokes and Isaacson, 2010; Suzuki and Bekkers, 2010). Following a given sensory stimulus train, differences in onset times of the AP-induced somatic Ca^{2+} transient therefore reflect the degree of a given cell's recruitment by sensory afferents.

Fast population TPCI at 125 Hz enabled us to identify the sequence of cells recruited in a train of synaptic stimulation (Fig. 13B and C). For a train of 5 layer 1a stimuli at 20 Hz, we analyzed the temporal sequence of AP-firing onset in layer II

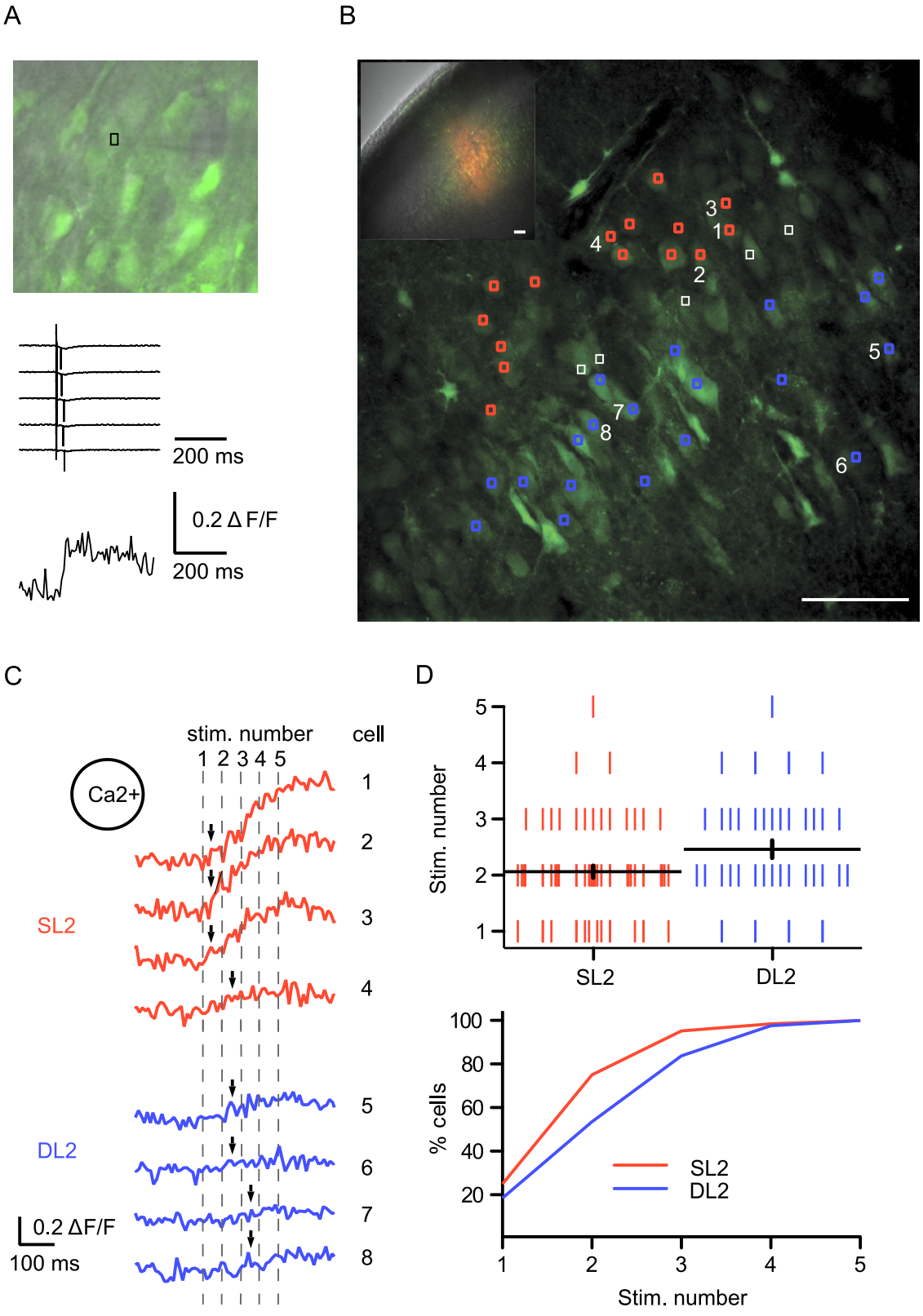
A
B
200 ms
0.2 Δ F/F
200 ms
3
1
4
2
5
7
8
6
C
stim. number
1 2 3 4 5
cell
Ca2+
1
2
SL2
3
4
5
DL2
6
7
8
0.2 ΔF/F
100 ms
D
Stim. number
5
4
3
2
1
SL2
DL2
% cells
100
80
60
40
20
SL2
DL2
1
2
3
4
5
Stim. number

Figure 13 *– Single cell excitability probing of sensory layer Ia inputs to deep and superficial layer II neurons by fast TPCI*

A Top: aPC bolus loaded with OG-BAPTA1-AM. Overlay of green fluorescence and transmitted infrared to visualize bolus-loaded cell and patch pipette. Black box indicates position of cell used for simultaneous cell-attached recording and Ca^{2+} imaging. Middle, five subsequent synaptically induced single APs measured in cell-attached patch underlying averaged Ca^{2+} transient in bottom panel.

B Inset: overlay of fluorescence and transmitted infrared (scale bars correspond to 50 µm). Main picture: High-magnification image of layer II neurons from inset. Numbers 1-8 label example cells corresponding to the traces in C. Blue boxes correspond to superficial layer 2 cells, white boxes correspond to cells neither attributable to superficial and deep half of rows (middle), red boxes correspond to cells in deep half of layer II cell rows (scale bar corresponds to 50 µm).

C Averaged Ca^{2+} traces evoked by extracellular electrical stimulation of layer Ia (layer Ib blocked by baclofen) inputs to superficial (red) and deep (blue) layer II cells as labelled in B. The vertical grey lines correspond to the timepoints each of the 5 pulses were delivered with an interpulse interval of 50 ms. Black arrows are placed in the stimulation interval in which the onset could be detected.

D Top: On average, superficial cells in layer II display the onset of averaged Ca^{2+} transients indicating AP firing after significantly less stimuli than deep cells in layer II (mean stimulus number 2.1 ±0.1 a.u. vs. 2.5 ±0.16 a.u., respectively; $p<0.05$, Mann-Whitney U Test). Bottom: Cumulative frequency of data displayed in top.

cell populations after isolated sensory afferent stimulation (Fig. 13C). We first determined the onset of each individual cell's somatic Ca^{2+} transient (for details, see Materials and Methods). In the combined cell-attached and Ca^{2+}-imaging experiments, single AP-mediated onsets of the Ca^{2+}-transients were detected in a temporal window of 10 to 30 ms after delivery of the synaptic stimulus. By analysing the onset time of the Ca^{2+}-transient, we could estimate the stimulus number in a train after which each individual cell started to display a suprathreshold response. For further analysis, cells were categorized according to the position of the responding cells along the vertical axis yielding two groups: Superficial layer II cells (SL2s, n=64/5/3 cells/slices/animals) and deep layer 2 cells (DL2s, n=43/5/3 cells/slices/animals; see Materials and Methods for further details). Note that by their definition these groups are not identical to the before defined L2S and L2P cells, however, as the intrinsic properties correspond to the cells position on the vertical axis (Fig. 7A), they should be comparable.

On average, in 20 Hz trains of five extracellular stimuli, SL2 cells exhibited an onset of the AP-mediated somatic Ca^{2+} transient after significantly less stimuli than DL2 cells (mean stimulus number 2.1 ±0.1 vs. 2.5 ±0.16; $p<0.05$, Mann-Whitney-U-test,

Fig. 13D). AP-firing in response to our specific train of sensory stimuli in aPC layer II cells thus occurs in a distinct temporal pattern: Superficial layer II cells respond earlier than deep layer II cells. This delay is probably underestimated based on the stronger hyperpolarizing effect of baclofen on SL cells (Suzuki and Bekkers, 2011). Under stimulus conditions presented here, the earlier recruitment of superficial cells by sensory inputs is consistent with the early predominant superficial cell activation seen in vivo with current source density analysis (Ketchum and Haberly, 1993).

7 DISCUSSION

Principal cells in the aPC display unique patterns of microcircuit design: Sensory and intracortical circuits activate different cells at different proportions, depending on their position along the superficial-to-deep gradient that also correlates with input resistance and burstiness of spiking: LSPS experiments show that intracortical connectivity gradually increases with the principal cell's position on the vertical axis from superficial to deep layers (Fig. 11B, C, and D), a higher burstiness and a lower input resistance. Fast two-photon population Ca^{2+} imaging of AP-mediated somatic Ca^{2+} transients in layer II evoked by selective layer Ia stimulation indicates stronger sensory recruitment of L2Ss (Fig. 13C and D).

7.1 Limitations

When interpreting connectivity studies in acute brain slice preparations using LSPS, one has to consider that the analysis is biased towards local axonal projections preserved in the slicing plane (Steriade, 2001). Morphological reconstructions of L2P cell axons did not reveal a predominant local projection pattern in the anterior-posterior axis as opposed to the dorsoventral axis (Johnson et al., 2000). We therefore chose the coronal slicing plane to analyse cell-type specific local intracortical circuitry in the dorsoventral axis.

The limitations of the connectivity-coefficient as a layer-specific measure of connectivity also need to be discussed. Different source cell types in different cortical layers display distinct response patterns to LSPS and cannot be segregated. LSPS cannot resolve the single presynaptic cell types in layer II. Single-cell-resolution connectivity mapping can be achieved using Ca^{2+}-imaging assisted identification of presynaptic cells selectively activated with 2P-uncaging (Nikolenko et al., 2007) or rabies-virus-dependent retrograde mono-trans-synaptic labeling (Miyamichi et al., 2010).

Glutamate uncaging results in a cell-type dependent amount of spatially adjacent suprathreshold hotspots that represent a single presynaptic cell. This makes it difficult to extract the specific stochiometry of presynaptic source- and

postsynaptic target cells (but see Bendels et al., 2010). We assume that LSPS samples identical populations of (presynaptic) source cells in a given layer and thus focus quantification of microcircuitry on layer-specific differences in the input pattern of identified target cells.

7.2 The organization of intracortical and sensory circuits in aPC layer II can be described as a converse gradient

A recent publication by Suzuki and Bekkers compared synaptic properties of preselected canonical L2S and L2P cells (Suzuki and Bekkers, 2011). Their results complement the findings from LSPS-mediated connectivity analysis and population Ca^{2+}-imaging presented here. L2P cells were shown to have strong layer 1b inputs then L2S, matching the increase of intracortical connectivity we observed when recording cells that were located deeper on the vertical axis in layer II. Suzuki and Bekkers found that L2S cells have strong 1a inputs and weak 1b inputs, consistent with their low intracortical connectivity found in our study. The more effective recruitment of superficial layer II cells by sensory activation we observed on the population level reflects the larger input strength of sensory synapses onto these cells.

When using cluster analysis of 22 intrinsic and morphological parameters, Suzuki and Bekkers draw the conclusion that layer II cells fall into two distinct groups. The functional analysis presented is then limited to a preselected subpopulation of canonical SL and SP cells (Suzuki and Bekkers, 2011). Our clustering approach operates on a much smaller number (3) of phenotypical parameters (including position). We thus cannot make statements about the distinctness of two cell groups with respect to functional microcircuit organization. We rather use clustering as a tool for aiding subsequent data analysis. Note that our cluster analysis generating two groups does neither confirm nor disprove the findings of Suzuki and Bekkers (2011), as one has to preselect the number of clusters before the analysis. In their discussion, Suzuki and Bekkers also hint at the possibility that the ‘distinction between SL and SP-cells might not always be clear cut‘ (Suzuki and Bekkers, 2011). Our results are also consistent with a continuous distribution of

cell phenotypes, though (see Fig. 3A and scatter plots in Fig. 3B). Most notably, our connectivity data correlates with the intrinsic cellular properties (Fig. 11B and C). We focus on the functional analysis of local associative microcircuitry of principals cells over the whole expanse of layer II and superficial layer III. This functional perspective rather supports the view of graded transitions of microcircuit patterns from sensory to intracortical for aPC projection neurons oriented along a vertical, superficial to deep axis (for summary, see Fig. 11A). Interestingly, in sensory neocortices sensory and associative inputs do not target all principle cells of a distinct layer to the same degree, but are organised in gradients, too (Shipp, 2007). However, as we have limited our analysis to a subset of factors defining a cell type, we cannot rule out with certainty that the observed functional gradient appears as a result of a superposition of several distinct cell populations.

7.3 Specialized superficial microcircuits

Our results imply that more superficial and less bursty layer II cells are receiving with respect to the stimulus earlier and stronger sensory inputs from M and T cells than cells that are located deeper and that show higher output burstiness. Conversely, deeper and burstier cells seem to be stronger integrated into intracortical associative microcircuits. Recently, Poo and Isaacson (2011) were able to show in vivo that for the strength of odour-evoked synaptic excitation recurrent associative connections play an important role. In their study, they distinguished cells that showed excitatory responses to a broad range of different odours (broadly tuned cells and cells that were responding only to a few specific odours (selectively tuned cells). Broadly and selectively tuned cells received nearly the same amount of excitation from sensory afferents, whereas the broadly tuned cells received a much stronger amount of intracortical association-mediated excitation. Poo and Isaacson claimed that all their recorded cells were pyramidal neurons and not semilunar cells. However, their criterion for classifying cells as pyramids was only the presence of basal dendrites. Our results suggest that this is not sufficient, as a gradient with many intermediate phenotypes between an extreme semilunar and an extreme pyramidal population seems to exist – and that

these intermediate cells do have basal dendrites (figure 5). One might therefore speculate, that the selectively tuned cells with a stronger integration in associative circuits correspond more to pyramidal-like neurons, the broadly tuned cells to semilunar-like cells. This view is supported by the reconstructed example cells shown in the paper, where the broadly tuned cell has only short basal dendrites and a V-like apical dendrite pair without a primary apical dendrite – a typical configuration of semilunar-pyramidal transition cells (Poo and Isaacson, 2011; for comparison see figure 5D).

The results from Suzuki and Bekkers (2011) as well as Poo and Isaacson (2011) together with our findings suggest that PC principal cell microcircuitry is organized in specialized subcircuits, integrating various proportions of sensory and intracortical associative inputs. This specialisation opens new options to shape incoming sensory information and permits for mechanisms like pattern separation and pattern completion by reinforcement or suppression of incoming sensory signal patterns (Wilson, 2011; Poo and Isaacson, 2011).

7.4 Output firing, cortical odour coding, plasticity

Our results suggest that olfactory cortex principal cells are integrated to various degrees in sensory and intracortical microcircuits. Therefore, sensory processing will be dominated by cells with intrinsic properties different from those mainly recruited by intracortical processing. An interesting parameter in this respect is the difference in burst index, i.e. spike frequency adaptation seen within layer II and layer III cells. For layer II cells, this difference in neuronal output mode has been speculated to play a role in olfactory coding (Suzuki and Bekkers, 2006). We propose that spike frequency adaptation of aPC projection neurons indicates to their postsynaptic partners their incorporation into sensory and/or intracortical microcircuits: Cells receiving a high proportion of sensory content will fire with lower spike frequency adaptation rates than cells activated by intracortical circuits. So far, the view of the PC as an association cortex is mainly based on studies not taking into account the distinct connectivity properties and output modes of cells (Schoenbaum and Eichenbaum, 1995; Johnson et al., 2000; Haberly, 2001; Calu et

al., 2007; Roesch et al., 2007; Stettler and Axel, 2009, Poo and Isaacsson, 2011). Further studies in vivo will have to determine if cells with different output modes differentially encode olfactory information.

Recently it was demonstrated that bursting is a prerequisite for the induction of plasticity in associative layer 1b synapses (Johenning et al., 2009). Bursts can be observed in vivo with a natural stimulation by olfactory stimuli, too (Wilson et al., 1998). aPC cells with high burst indexes also display initial bursts firing at high frequencies (Suzuki and Bekkers, 2006). As the incorporation into the local circuitry is related to a principal cell's burst index, we propose that bursting and the related spike frequency adaptation may be an intrinsic mechanism not only relevant for odour encoding but also synaptic plasticity and odour learning. Burstiness may therefore indicate stronger intracortical connectivity and promote plasticity of intracortical synapses. This could result in a cell's output mode determining the degree of intracortical connectivity.

7.5 Intracortical connections along the dorso-ventral axis: Asymmetry and the role of deep cells

The aPC has been divided into different subregions with unknown functional differences along the dorsoventral axis (Ekstrand et al., 2001). On this axis, L3P inputs display a significant asymmetric dorsal shift of their deep layer III inputs (Fig. 12B). aPC inhibitory inputs to pyramidal cells are also asymmetrically organized with a posterior shift on the anterior-posterior axis (Luna and Pettit, 2010). The concept of layer-specific asymmetric local excitatory connections from deeper layers has recently been in the focus of studies in auditory (Oviedo et al., 2010) and medial entorhinal cortex (Beed et al., 2010), with interesting computational implications in these areas. In layer III, there is a superficial to deep shift of phenotype from pyramidal to excitatory multipolar cells (Neville and Haberly, 2004). More pronounced in the dorsal then in the ventral part of the aPC, the endopiriform nucleus (or layer IV) is located deep to layer III. It contains no pyramidal but only multipolar cells (Tseng and Haberly et al., 1989a). It is tempting to speculate that the observed asymmetry is due to specific projection patterns of

multipolar cells onto L3Ps (see also Fig. 12D), and recalls the importance to take into consideration the deep layers as well, when conceiving network models of the PC.

7.6 An updated (and speculative) PC network model

Integrating the new results from Suzuki and Bekkers (2010 and 2011) and our group (Wiegand et al. 2011), what would an updated PC network model look like?
Sensory inputs from the OB M and T cells arrive the PC via the LOT. They synapse in layer Ia on dendrites of excitatory principle cells and feedforward inhibitory interneurons, mainly horizontal cells. These inhibitory interneurons exercise a "global" inhibition about the largest part of the excitatory cell population (together with layer III feedback interneurons). The excitatory cells are not a homogenous population: In layer II they are organised following a gradient on the superficial to deep axis between an extreme semilunar population at the border to layer I and an extreme pyramidal population at the border to layer III (Fig. 14).
The more semilunar-like a cell is, the more and earlier it receives sensory inputs and the lesser associative inputs (Fig. 14A). Probably it is tuned to a broad range of odours (Poo and Isaacson, 2011). By an elegant tissue cut experiment Suzuki and Bekkers (2011) could show in a different experimental setting both that semilunar-like cells receive earlier and more sensory inputs and that they are connected to layer II pyramidal-like cells. In a recent publication they revealed these neurons are more than pyramidal like cells implied in driving fast-spiking inhibitory multipolar cells (Suzuki and Bekkers, 2012). Thus one of their functions might be to drive more pyramidal like cells. Another function might be to mediate the 'gobal' or general inhibition that can be observed in in vivo experiments (Poo and Isaacson, 2009; Stettler and Axel, 2009; Suzuki and Bekkers, 2012) and that might allow a more precise odour processing by the few activated deeper pyramidal like cells. However, many questions about this cell population remain open: Why does sensory information does not reach the more pyramidal like population directly? What is this additional processing step of sensory information by semilunar-like cells good for? What is their in vivo firing behaviour (as in most in vivo studies only

pyramidal cells were identified)? How are they connected to deep pyramidal cells? When and supported by which factors in development the cells form the different subcircuits?

The deeper and the more pyramidal-like a cell is, the stronger it is integrated into local associative microcircuits and receives lesser, later and narrower tuned sensory inputs. L2P and L3P can undergo long-term plasticity (LTP and LTD) on their associative input sites. Their main output pattern consists of bursts of action potentials. Output bursts that are precisely (spike-) timed to dendritic input are a prerequisite for inducing long-term potentiation. Furthermore, the local associative circuits allow boosting excitatory responses (Poo and Isaacson, 2011). Maybe in concert with feedback inhibitory interneurons like fast-spiking inhibitory multipolar cells (Suzuki and Bekkers, 2012), which could provide lateral inhibition mechanisms, contrasts could be sharpened. This allows a precise but flexible odour coding. By these plasticity-, activation- and suppression-capacities, this pyramidal like cell population seems to be well suited to serve as a dynamic memory system with functions like pattern separation, pattern completion and discrimination learning (Leibold and Bendels, 2009).

Firing patterns in the aPC and pPC during behavioural tasks (Calu et al., 2007; Roesch et al., 2007; Schoenbaum and Eichenbaum, 1995), in vivo population Ca^{2+} imaging (Stettler and Axel, 2009) and morphometry of axonal projection patterns of neighbouring layer II pyramidal cells in the PC (Johnson et al., 2000) are compatible with the characteristic features of an association cortex. However, Suzuki and Bekkers (2011) study and our results show that a part of the cell population is specialized in feedforward processing of sensory information from the OB. As a consequence, this supports a model of the PC as a hybrid recurrent/feedforward pattern correlation network, as it had been put forward e.g. by Haberly (2001). The different but overlapping layers of sensory and associative processing make the PC appear closer to the canonical design of sensory neocortices (considering only the inputs, as not much is known about the wiring of both PC and neocortical outputs), where layer 4 principle cells are the first activated by ascending inputs (sensory inputs from the thalamus or from “lower” areas), next layer 3 principle neurons are activated by layer 4 cells, and a lower

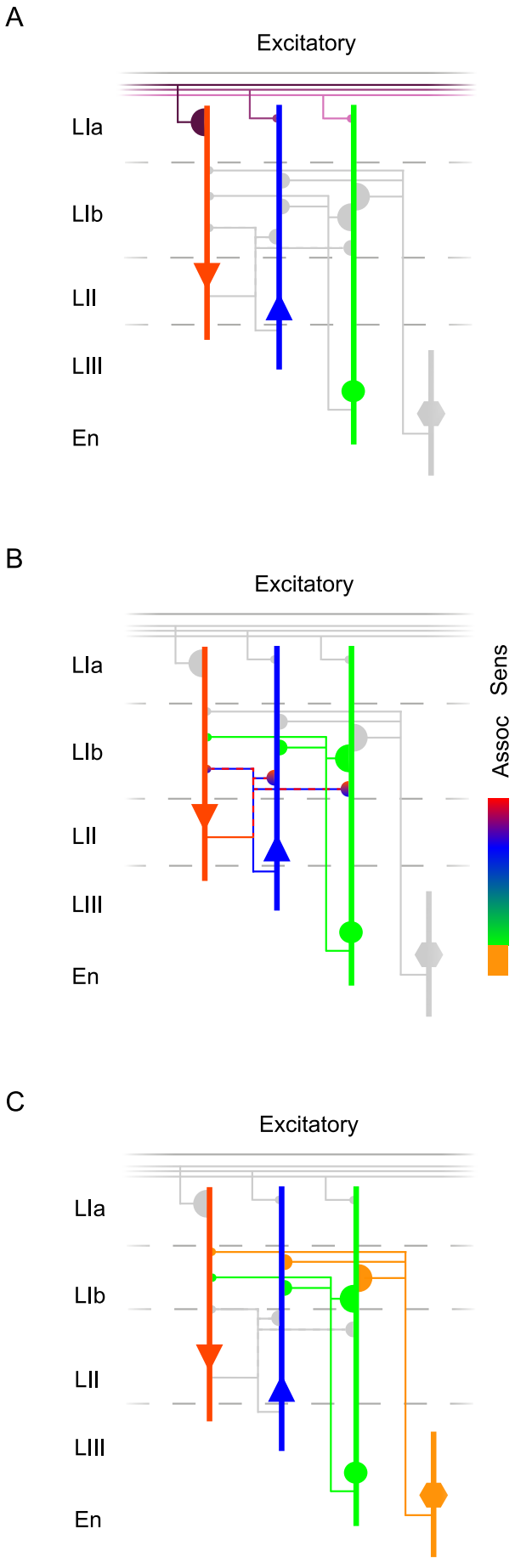
A
Excitatory
LIa
LIb
LII
LIII
En
B
Excitatory
LIa
LIb
LII
LIII
En
Sens
Assoc
C
Excitatory
LIa
LIb
LII
LIII
En

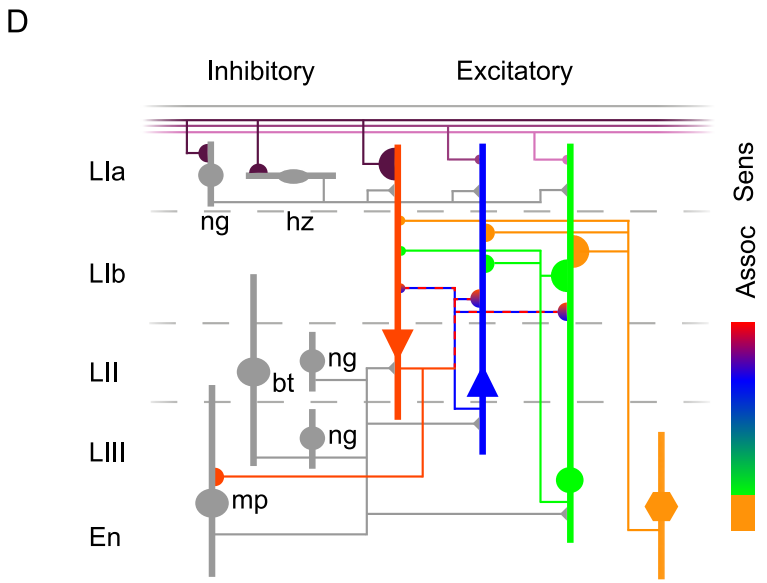

Figure 14 *– Schematic aPC circuit diagram*

A Sensory input via the LOT (violet lines) is projected to the L2S (red downward triangle), L2P (blue upright triangle) and L3P (green upright triangle) via synapses (violet semicircle) in Layer Ia. The radius of the discs indicates the input strength. The coloured vertical bars indicate the dendrites of the respective cell types. More L2S like cells receive earlier, heavier and probably less specific sensory inputs then L2P and (probably) L3P like cells.

B The strength of the intracortical connections (coloured semicircles) is arranged in a superficial to deep gradient complementing sensory input strength. The deeper a cell lays on the superficial to deep axis, the more it is integrated into local associative circuits. Small coloured lines thereby indicate the axons. Note that LSPS does not allow distinguishing between L2S and L2P pyramidal cell inputs (red and blue circles).

C All cells receive heavy deep inputs, the deeper a cell lays on the superficial to deep axis, the stronger these inputs are. It is unclear if these inputs originate from L3P (green triangle) or L3M (orange hexagon) cells. The intracortical projection strength (green and orange lines and discs) from these deep cells follows the same gradient as the L2S/L2P projections (blue, red). The strong synaptic pathway from the deep cells to L3P cells exhibits a spatial asymmetry in that most of these projections arise from cells located more dorsally than the L3P.

D The integrated wiring diagram, including the known interneuron populations: layer I and II horizontal and neuroglomerular cells are implied in early feedforward inhibition, layer III fastspiking inhibitory multipolar cells in late perisomatic inhibition driven by L2S cells. The role of layer II and III regular spiking multipolar cells, neurogliaform cells and basket cells remains unclear.

proportion of sensory/ascending inputs is targeting directly layer 3. Descending corticocortical inputs target more superficial cells (in layer 2/3) via fibers in layer I, and deep layer 5/6 cells directly in the deep layers (Douglas and Martin, 2004; Shipp, 2007). A hypothesis would be that PC L2S correspond to layer 4 principle cells, L2P to layer 3 principle cells and PC deep cells to layer 5/6 cells.

In our study, all examined excitatory cell types receive heavy inputs from these deep layer III and endopiriform nucleus cells, so probably from L3P and L3M. This raises interesting questions: How do the inputs and targets of these two populations of excitatory neurons differ? What are their different functions? Do these inputs have the same function as local layer 2 connections, that seem to serve at least partially in boosting (Poo and Isaacson, 2011) or suppressing activation (lateral inhibition, Poo and Isaacson, 2009)? Or is one or are both of the populations a source of the oscillatory activity described in the literature that may serve to synchronize activity and to modulate activity states (see chapter 1.3.6; Murakami et al., 2005; Sanchz-Vives et al., 2008; Hasselmo and Bower, 1992; Wilson, 2010)?

The principle findings discussed in this chapter show how studies of functional microcircuitry can be a part in the puzzle that explains observations made by behavioural and imaging studies, e.g. the formation of odour objects in the olfactory cortex. In this way these functional studies on a cellular level help to understand how a sensory system is working.

8 SUMMARY/ABSTRACT

The Piriform Cortex (PC) is the largest component of the olfactory cortex. An anterior (aPC) and a posterior subdivision (pPC) can be distinguished. The PC has a three-layered horizontal organisation. Layer II and III principal excitatory cells in the aPC receive sensory inputs from the olfactory bulb and intracortical associative inputs from the PC itself and from other cortical region. We characterize organization principles of excitatory sensory and local intracortical associative microcircuits in acute slices of rat aPC using laser scanning photostimulation (LSPS) and fast two-photon population Ca^{2+} imaging (TPCI).

Layer II and III principal cells can be classified on a superficial-to-deep vertical axis. The position on this axis correlates with input resistance and bursting behaviour. LSPS experiments show that local intracortical connectivity gradually increases with the principal cell's position on the vertical axis from superficial to deep layers, and thus correlates with a higher burstiness and a lower input resistance. Fast TPCI of action potential-mediated somatic Ca^{2+} transients in layer II evoked by selective layer Ia stimulation indicates stronger sensory recruitment of the more superficial cells. Thus, in layer II, sensory circuits dominate superficial cells, whereas incorporation in intracortical circuits increases with depth. Additionally we analyzed the distribution of associative inputs along the dorsoventral axis. The intracortical layer III pyramidal cell inputs show an asymmetric dorsal offset.

The gradual functional specialisation of aPC principal cells in sensory feedforward or associative recurrent microcircuits supports a model of the PC as a hybrid recurrent/feedforward pattern correlation network, as it had been put forward e.g. by Haberly (2001). Furthermore, the different but overlapping layers of sensory and associative processing make the PC appear closer to the canonical design of sensory neocortices.

9 LITERATURE

Ambros-Ingerson J, Granger R, Lynch G (1990) Simulation of paleocortex performs hierarchical clustering. Science 247:1344–1348

Apicella A, Yuan Q, Scanziani M, Isaacson JS (2010) Pyramidal Cells in Piriform Cortex Receive Convergent Input from Distinct Olfactory Bulb Glomeruli. J Neurosci 30:14255–14260

Atanasova B, Graux J, Hage El W, Hommet C, Camus V, Belzung C (2008) Olfaction: a potential cognitive marker of psychiatric disorders. Neuroscience and biobehavioral reviews 32:1315–1325

Baba T, Kikuchi A, Hirayama K, Nishio Y, Hosokai Y, Kanno S, Hasegawa T, Sugeno N, Konno M, Suzuki K, Takahashi S, Fukuda H, Aoki M, Itoyama Y, Mori E, Takeda A (2012) Severe olfactory dysfunction is a prodromal symptom of dementia associated with Parkinson's disease: a 3 year longitudinal study. Brain, 135:161–169

Barkai E, Bergman RE, Horwitz G, Hasselmo ME (1994) Modulation of associative memory function in a biophysical simulation of rat piriform cortex. J Neurophysiol 72:659–677

Barnes DC, Hofacer RD, Zaman AR, Rennaker RL, Wilson DA (2008) Olfactory perceptual stability and discrimination. Nat Neurosci 11:1378–1380

Beed P, Bendels MHK, Wiegand HF, Leibold C, Johenning FW, Schmitz D (2010) Analysis of excitatory microcircuitry in the medial entorhinal cortex reveals cell-type-specific differences. Neuron 68:1059–1066

Bendels MHK, Beed P, Leibold C, Schmitz D, Johenning FW (2008) A novel control software that improves the experimental workflow of scanning photostimulation experiments. J Neurosci Methods 175:44–57

Bendels MHK, Beed P, Schmitz D, Johenning FW, Leibold C (2010) Detection of input sites in scanning photostimulation data based on spatial correlations. J Neurosci Methods

Best AR, Thompson JV, Fletcher ML, Wilson DA (2005) Cortical metabotropic glutamate receptors contribute to habituation of a simple odor-evoked behavior. J Neurosci 25:2513–2517

Best AR, Wilson DA (2004) Coordinate synaptic mechanisms contributing to olfactory cortical adaptation. J Neurosci 24:652–660

Brunjes PC, Illig KR, Meyer EA (2005) A field guide to the anterior olfactory nucleus (cortex). Brain Res Brain Res Rev 50:305–335

Calu DJ, Roesch MR, Stalnaker TA, Schoenbaum G (2007) Associative encoding in posterior piriform cortex during odor discrimination and reversal learning. Cereb Cortex 17:1342–1349

Chiovini B, Turi GF, Katona G, Kaszás A, Erdélyi F, Szabó G, Monyer H, Csákányi A, Vizi ES, Rózsa B (2010) Enhanced dendritic action potential backpropagation in parvalbumin-positive basket cells during sharp wave activity. Neurochem. Res. 35:2086–2095

Chu S, Downes JJ (2000) Long live Proust: the odour-cued autobiographical memory bump. Cognition 75:B41–50

De Felipe J, Jones EG (2010) Neocortical microcircuits. In: Handbook of brain microcircuits, Ed 1 (Shepherd GM, Grillner S, eds), pp 5–14. New York: Oxford UP.

Douglas RJ, Martin KAC (2010) Canonical cortical circuits. In: Handbook of brain microcircuits, Ed 1 (Shepherd GM, Grillner S, eds), pp 15–21. New York: Oxford UP.

Douglas RJ, Martin KAC (2004) Neuronal Circuits of the Neocortex. Annu Rev Neurosci 27:419–451

Dunfield D, Haas K (2009) Metaplasticity Governs Natural Experience-Driven Plasticity of Nascent Embryonic Brain Circuits. Neuron 64:240–250

Dunfield D, Haas K (2010) In vivo single-cell excitability probing of neuronal ensembles in the intact and awake developing Xenopus brain. Nature Protocols 5:849–856

Ekstrand JJ, Domroese ME, Johnson DM, Feig SL, Knodel SM, Behan M, Haberly LB (2001) A new subdivision of anterior piriform cortex and associated deep nucleus with novel features of interest for olfaction and epilepsy. J Comp Neurol 434:289–307

Franks KM, Isaacson JS (2005) Synapse-specific downregulation of NMDA receptors by early experience: a critical period for plasticity of sensory input to olfactory cortex. Neuron 47:101–114

Gottfried JA (2010) Central mechanisms of odour object perception. Nat Rev Neurosci 11:628–641

Haberly LB (1983) Structure of the piriform cortex of the opossum. I. Description of neuron types with Golgi methods. J Comp Neurol 213:163–187

Haberly LB (2001) Parallel-distributed processing in olfactory cortex: new insights from morphological and physiological analysis of neuronal circuitry. Chem Senses 26:551–576

Haberly LB, Price JL (1978) Association and commissural fiber systems of the olfactory cortex of the rat. J Comp Neurol 178:711–740

Harris JC (2010) Camillo Golgi, nobel laureate: the olfactory bulb. Arch Gen Psychiatry 67:983–984

Hasselmo ME, Bower JM (1992) Cholinergic suppression specific to intrinsic not afferent fiber synapses in rat piriform (olfactory) cortex. J Neurophysiol 67:1222–1229

Herting B, Bietenbeck S, Scholz K, Hähner A, Hummel T, Reichmann H (2008)

[Olfactory dysfunction in Parkinson's disease: its role as a new cardinal sign in early and differential diagnosis]. Nervenarzt 79:175–184

Hoffman WH, Haberly LB (1991) Bursting-induced epileptiform EPSPs in slices of piriform cortex are generated by deep cells. J Neurosci 11:2021–2031

Hoffman WH, Haberly LB (1993) Role of synaptic excitation in the generation of bursting-induced epileptiform potentials in the endopiriform nucleus and piriform cortex. J Neurophysiol 70:2550–2561

Illig KR, Eudy JD (2009) Contralateral projections of the rat anterior olfactory nucleus. J Comp Neurol 512:115–123

Illig KR, Haberly LB (2003) Odor-evoked activity is spatially distributed in piriform cortex. J Comp Neurol 457:361–373

Isaacson JS (2010) Odor representations in mammalian cortical circuits. Curr Opin Neurobiol

Johenning FW, Beed PS, Trimbuch T, Bendels MHK, Winterer J, Schmitz D (2009) Dendritic Compartment and Neuronal Output Mode Determine Pathway-Specific Long-Term Potentiation in the Piriform Cortex. J Neurosci 29:13649–13661

Johenning FW, Holthoff K (2007) Nuclear calcium signals during L-LTP induction do not predict the degree of synaptic potentiation. Cell Calcium 41:271–283

Johnson DM, Illig KR, Behan M, Haberly LB (2000) New features of connectivity in piriform cortex visualized by intracellular injection of pyramidal cells suggest that "primary" olfactory cortex functions like “association” cortex in other sensory systems. J Neurosci 20:6974–6982

Jung MW, Larson J, Lynch G (1990) Long-term potentiation of monosynaptic EPSPs in rat piriform cortex in vitro. Synapse 6:279–283

Kanter ED, Haberly LB (1990) NMDA-dependent induction of long-term potentiation in afferent and association fiber systems of piriform cortex in

vitro. Brain Res 525:175–179

Kanter ED, Haberly LB (1993) Associative long-term potentiation in piriform cortex slices requires GABAA blockade. J Neurosci 13:2477–2482

Kaupp UB (2010) Olfactory signalling in vertebrates and insects: differences and commonalities. Nat Rev Neurosci 11:188–200

Ketchum KL, Haberly LB (1993) Membrane currents evoked by afferent fiber stimulation in rat piriform cortex. I. Current source-density analysis. J Neurophysiol 69:248–260

Lazarini F, Lledo P-M (2011) Is adult neurogenesis essential for olfaction? Trends Neurosci 34:20–30

Leibold C, Bendels MH (2009) Learning to discriminate through long-term changes of dynamical synaptic transmission. Neural Comput 21: 3408 –3428

Li W, Howard JD, Gottfried JA (2010) Disruption of odour quality coding in piriform cortex mediates olfactory deficits in Alzheimer's disease. Brain 133:2714–2726

Liberini P, Parola S, Spano PF, Antonini L (2000) Olfaction in Parkinson's disease: methods of assessment and clinical relevance. J Neurol 247:88–96

Lorincz A, Rozsa B, Katona G, Vizi ES, Tamas G (2007) Differential distribution of NCX1 contributes to spine-dendrite compartmentalization in CA1 pyramidal cells. Proc Natl Acad Sci U S A 104:1033–1038.

Luna VM, Pettit DL (2010) Asymmetric rostro-caudal inhibition in the primary olfactory cortex. Nat Neurosci

Luna VM, Schoppa NE (2008) GABAergic circuits control input-spike coupling in the piriform cortex. J Neurosci 28:8851–8859

McIntyre DC and Gilby KL (2008) Mapping seizure pathways in the temporal lobe. Epilepsia 49: 23-30

Malenka RC & Nicoll RA (1997) Learning and memory. Never fear, LTP is hear. Nature 390: 552–553

Manabe H, Kusumoto-Yoshida I, Ota M, Mori K (2011) Olfactory cortex generates synchronized top-down inputs to the olfactory bulb during slow-wave sleep. J Neurosci 31:8123–8133

Miyamichi K, Amat F, Moussavi F, Wang C, Wickersham I, Wall NR, Taniguchi H, Tasic B, Huang ZJ, He Z, Callaway EM, Horowitz MA, Luo L (2011) Cortical representations of olfactory input by trans-synaptic tracing. Nature 472:191–196

Mori K, Nagao H, Yoshihara Y (1999) The olfactory bulb: coding and processing of odor molecule information. Science 286:711–715

Murakami M, Kashiwadani H, Kirino Y, Mori K (2005) State-dependent sensory gating in olfactory cortex. Neuron 46:285–296

Murthy VN (2011) Olfactory Maps in the Brain. Annu Rev Neurosci 34:233–258

Nagao H, Yamaguchi M, Takahash Y, Mori K (2002) Grouping and representation of odorant receptors in domains of the olfactory bulb sensory map. Microsc Res Tech 58:168–175

Neville KR, HaberlyLB (2004) Olfactory cortex. In: The synaptic organization of the brain, Ed 5 (Shepherd GM, ed), pp 415– 454. New York: Oxford UP

Nikolenko V, Poskanzer KE, Yuste R (2007) Two-photon photostimulation and imaging of neural circuits. Nat. Methods 4:943–950

Oviedo HV, Bureau I, Svoboda K, Zador AM (2010) The functional asymmetry of auditory cortex is reflected in the organization of local cortical circuits. Nat Neurosci 13:1413–1420

Poo C & Isaacson JS (2007) An early critical period for long-term plasticity and structural modification of sensory synapses in olfactory cortex. J Neurosci 27: 7553–7558

Poo C, Isaacson JS (2009) Odor Representations in Olfactory Cortex: “Sparse” Coding, Global Inhibition, and Oscillations. Neuron 62:850–861

Poo, C, & Isaacson, JS (2011) A Major Role for Intracortical Circuits in the Strength and Tuning of Odor-Evoked Excitation in Olfactory Cortex. Neuron, 72:41–48

Popper, K (2002) The Logic of Scientific Discovery. London, New York: Taylor and Francis

Quinlan EM, Lebel D, Brosh I, Barkai E (2004) A molecular mechanism for stabilization of learning-induced synaptic modifications. Neuron 41:185–192

Rennaker RL, Chen C-FF, Ruyle AM, Sloan AM, Wilson DA (2007) Spatial and temporal distribution of odorant-evoked activity in the piriform cortex. J Neurosci 27:1534–1542

Roesch MR, Stalnaker TA, Schoenbaum G (2007) Associative encoding in anterior piriform cortex versus orbitofrontal cortex during odor discrimination and reversal learning. Cereb Cortex 17:643–652

Rogan MT, Stäubli UV & LeDoux JE (1997) Fear conditioning induces associative long-term potentiation in the amygdala. Nature, 390: 604–607

Sanchez-Vives MV, Descalzo VF, Reig R, Figueroa NA, Compte A, Gallego R (2008) Rhythmic spontaneous activity in the piriform cortex. Cereb Cortex 18:1179–1192

Schoenbaum G, Eichenbaum H (1995) Information coding in the rodent prefrontal cortex. I. Single-neuron activity in orbitofrontal cortex compared with that in pyriform cortex. J Neurophysiol 74:733–750

Shepherd GMG, Pologruto TA, Svoboda K (2003) Circuit analysis of experience-dependent plasticity in the developing rat barrel cortex. Neuron 38:277–289

Shipley MT, Ennis M (1996) Functional organization of olfactory system. J Neurobiol 30:123–176

Shipp S (2007) Structure and function of the cerebral cortex. Current Biology 17:R443–R449

Smetters D, Majewska A, Yuste R (1999) Detecting action potentials in neuronal populations with calcium imaging. Methods 18:215–221

Steriade M (2001) The intact and sliced brain. Cambridge, MA: MIT

Stettler DD, Axel R (2009) Representations of Odor in the Piriform Cortex. Neuron 63:854–864

Stokes CCA, Isaacson JS (2010) From dendrite to soma: dynamic routing of inhibition by complementary interneuron microcircuits in olfactory cortex. Neuron 67:452–465

Stosiek C, Garaschuk O, Holthoff K, Konnerth A (2003) In vivo two-photon calcium imaging of neuronal networks. Proc Natl Acad Sci USA 100:7319–7324

Sugai T, Miyazawa T, Fukuda M, Yoshimura H, Onoda N (2005) Odor-concentration coding in the guinea-pig piriform cortex. Neuroscience 130:769–781

Süßkind P (1987) Das Parfüm. Zürich: Diogenes Verlag

Suzuki N, Bekkers JM (2006) Neural coding by two classes of principal cells in the mouse piriform cortex. J Neurosci 26:11938–11947

Suzuki N, Bekkers JM (2010) Distinctive Classes of GABAergic Interneurons Provide Layer-Specific Phasic Inhibition in the Anterior Piriform Cortex. Cereb Cortex

Suzuki N, Bekkers JM (2011) Two layers of synaptic processing by principal neurons in piriform cortex. J Neurosci 31: 2156–2166

Suzuki N, Bekkers JM (2012) Microcircuits Mediating Feedforward and Feedback Synaptic Inhibition in the Piriform Cortex. J Neurosci 32:919 - 931

Tang AC, Hasselmo ME (1994) Selective suppression of intrinsic but not afferent

fiber synaptic transmission by baclofen in the piriform (olfactory) cortex. Brain Res 659:75–81

Treves A, Rolls ET (1992) Computational constraints suggest the need for two distinct input systems to the hippocampal CA3 network. Hippocampus 2:189–199

Tseng GF, Haberly LB (1989a) Deep neurons in piriform cortex. I. Morphology and synaptically evoked responses including a unique high-amplitude paired shock facilitation. J Neurophysiol 62:369–385

Tseng GF, Haberly LB (1989b) Deep neurons in piriform cortex. II. Membrane properties that underlie unusual synaptic responses. J Neurophysiol 62:386–400

Wattendorf E, Welge-Lüssen A, Fiedler K, Bilecen D, Wolfensberger M, Fuhr P, Hummel T, Westermann B (2009) Olfactory impairment predicts brain atrophy in Parkinson's disease. J Neurosci 29:15410–15413

Wesson DW, Levy E, Nixon RA, Wilson DA (2010) Olfactory Dysfunction Correlates with Amyloid- Burden in an Alzheimer's Disease Mouse Model. J Neurosci 30:505–514

Wiegand HF, Beed P, Bendels MHK, Leibold C, Schmitz D, Johenning FW (2011) Complementary sensory and associative microcircuitry in primary olfactory cortex. J Neurosci 31:12149–12158

Wiegand HF, Schmitz D, Johenning FW (2010) Metabotropic glutamate receptors and presynaptic calcium in olfactory cortical adaptation. FENS Abstr., vol.5, 014.42

Wilson DA (1998) Habituation of Odor Responses in the Rat Anterior Piriform Cortex. J Neurophysiol 79:1425-1440

Wilson DA (2010) Single-Unit Activity in Piriform Cortex during Slow-Wave State Is Shaped by Recent Odor Experience. J Neurosci 30:1760–1765

Wilson DA, Kadohisa M, Fletcher ML (2006) Cortical contributions to olfaction: plasticity and perception. Semin Cell Dev Biol 17:462–470

Wilson DA, Yan X (2010) Sleep-like States modulate functional connectivity in the rat olfactory system. J Neurophysiol 104:3231–3239

Yang J, Ul Quraish A, Murakami K, Ishikawa Y, Takayanagi M, Kakuta S, Kishi K (2004) Quantitative analysis of axon collaterals of single neurons in layer IIa of the piriform cortex of the guinea pig. J Comp Neurol 473:30–42

Yeshurun Y, Lapid H, Dudai Y, Sobel N (2009) The Privileged Brain Representation of First Olfactory Associations. Current Biology 19:1869–1874

Young A, Sun Q-Q (2007) Long-term modifications in the strength of excitatory associative inputs in the piriform cortex. Chem Senses 32:783–794

10 SELBSTÄNDIGKEITSERKLÄRUNG

Autorenschaft dieser Arbeit:

Ich, Hauke Wiegand, erkläre, dass ich die vorgelegte Dissertation mit dem Thema: „Sensory and associative microcircuits in the olfactory cortex“ selbst verfasst und keine anderen als die angegebenen Quellen und Hilfsmittel benutzt, ohne die (unzulässige) Hilfe Dritter verfasst und auch in Teilen keine Kopien anderer Arbeiten dargestellt habe.
Der ‘Methods’ und der ‘Results’-Teil dieser Arbeit sowie die Abbildungen 5 bis 13 wurden modifiziert aus dem von mir mitverfassten Paper “Complementary sensory and associative microcircuitry in primary olfactory cortex “ (Wiegand et al., 2011) übernommen.

Durchführung und Auswertung der Experimente:

Die LSPS-Experimente wurden zum Großteil von mir selber durchgeführt, Friedrich Johenning hat mich bei der Arbeit unterstützt. Ich habe diese Experimente selber ausgewertet, Software und Allgorythmen dazu wurden von Michael Bendels programmiert und von Prateep Beed angepasst. Die Zwei-Photonen-Experimente wurden von Friedrich Johenning durchgeführt, ich habe ihn bei der Arbeit unterstützt. Diese Experimente wurden von Friedrich Johenning ausgewertet. Die Färbungen wurden von Susanne Walden bearbeitet und von mir ausgewertet.

Berlin, den 01.08.2012

11 CURRICULUM VITAE

Mein Lebenslauf wird aus datenschutzrechtlichen Gründen in der elektronischen Version meiner Arbeit nicht veröffentlicht.

12 PUBLIKATIONEN UND POSTER

Publikationen

Beed P, Bendels MHK, Wiegand HF, Leibold C, Johenning FW, Schmitz D (2010) Analysis of excitatory microcircuitry in the medial entorhinal cortex reveals cell-type-specific differences. Neuron 68:1059–1066.

Wiegand HF, Beed P, Bendels MHK, Leibold C, Schmitz D, Johenning FW (2011) Complementary sensory and associative microcircuitry in primary olfactory cortex. J Neurosci 31:12149–12158.

Poster

Beed P, Bendels M, Wiegand HF, Leibold C, Johenning F, Schmitz D (2009) Microcircuitry in the medial entorhinal cortex reveals a cell-type–specific and modular organization. 39th Annual Meeting of the Society for Neuroscience. Chicago, USA.

Wiegand HF, Schmitz D and Johenning FW (2010) Metabotropic glutamate receptors and presynaptic calcium in olfactory cortical adaptation. FENS Abstr., vol.5, 014.42.